Ore Geology Reviews 92 (2018) 297–317

Contents lists available at ScienceDirect

Ore Geology Reviews

journal homepage: www.elsevier.com/locate/oregeorev

Chlorite, white mica and clay minerals as proximity indicators to ore in the shallow porphyry environment of Quebrada de la Mina deposit, Argentina

Laura Maydagán[a,b,*], Marta Franchini[a,c,d], Agnes Impiccini[d], David Lentz[e], Patricia Patrier[f], Daniel Beaufort[f]

[a] Centro Patagónico de Estudios Metalogenéticos-CONICET, Argentina
[b] INGEOSUR-CONICET, Departamento de Geología, Universidad Nacional del Sur, Av. Alem 1253, Cuerpo B', 8000 Bahía Blanca, Argentina
[c] Instituto de Investigación en Paleobiología y Geología, Universidad Nacional de Río Negro, Av. Roca 1242, 8332 Roca, Argentina
[d] Departamento de Geología y Petróleo, Facultad de Ingeniería, Universidad Nacional del Comahue, Buenos Aires 1400, 8300 Neuquén, Argentina
[e] Department of Earth Sciences, University of New Brunswick, Fredericton, New Brunswick E3B 5A3, Canada
[f] IC2MP, HydrASA, Université de Poitiers, CNRS–UMR 7285, 6 rue M. Brunet, TSA 51106, F-86073 Poitiers Cedex 9, France

ARTICLE INFO

Keywords:
Porphyry deposit
Clays
Phyllosilicates
Hydrothermal assemblages

ABSTRACT

The mineralogy and chemical composition of mica-like phyllosilicates (> 2 μm) and clay fraction (< 2 μm) of the shallow hydrothermal alteration zones of the Quebrada de la Mina Cu-Au deposit (San Juan Province, Argentina) were constrained by petrography, XRD, electronic microprobe and IR. The results allow us to identify: (1) relict patches of quartz + K-feldspar ± rutile (potassic) alteration, (2) a peripheral clinochlore-rich propylitic halo, and (3) a central white mica (> 2 μm) and illite halo associated with phyllic and tourmaline-rich phyllic assemblages.

The subhorizontal, shallow level Au-rich (> 0.5 ppm Au) zone at the Quebrada de la Mina deposit coincides with the phyllic halo. The distribution of Au, Ag, Zn, Pb and As forms partially overlapping haloes toward shallower levels. Weak Cu (Mo) anomalies were found in potassic patches below the Au-rich zone. High Mn and Fe contents in clinochlore from the peripheral propylitic halo suggest a distance of ~1 km to a porphyry Cu-(Au) mineralized core at deeper levels.

White micas (> 2 μm) in Quebrada de la Mina show a range of compositions between muscovite and illite. In the propylitic halo and in the patches of potassic alteration, white micas (> 2 μm) show the highest values of Fe + Mg + Mn (0.40–0.55 apfu) and the lowest of Al (2.40–2.55 apfu). In the phyllic alteration zone of Quebrada de la Mina, white micas (> 2 μm) with Al contents between 2.45 and 2.70 apfu and Fe + Mg + Mn between 0.35 and 0.15 apfu match the areas with high gold content (> 0.5 ppm Au). The lowest values of Fe + Mg + Mn (0.11–0.05 apfu) and the highest Al contents (2.80–2.85 apfu) occur in white micas from the tourmaline-rich phyllic zone.

Values of the Kübler index of illite of 0.19–0.1 2θ in the clay fraction of deep samples are indicative of higher temperature and/or higher fluid/rock ratios during illite formation, compared to values of the Kübler index > 0.2 2θ recognized in shallow samples. Thus, both the compositional variations in chlorite and white micas and the illite crystallinity could be used as a guide for exploration of copper-gold mineralization in shallow levels of porphyry systems.

1. Introduction

Early studies of porphyry copper systems have used the geochemical and mineralogical zoning patterns of these deposits as a footprint guide for exploration (e.g., Meyer and Hemley, 1967; Lowell and Guilbert, 1970; Gustafson and Hunt, 1975; Dilles and Einaudi, 1992). The illite Kübler index (KI; Guggenheim et al., 2002) has been used to delineate paleothermal gradients in the southwestern Gaspé porphyry Cu deposit, Quebec (Duba and William-Jones, 1983; Williams-Jones, 1986), and as an indicator of mineralization in the Dexing porphyry Cu deposits, east China (In et al., 2002) and Campana Mahuida, Argentina (Franchini et al., 2007). White mica compositions have been used to map fluid pH gradients in porphyry deposits (e.g., Cohen, 2011). Recent studies showed that phyllosilicates are enriched in trace elements along vertical pathways of the magmatic hydrothermal plume extending from the ore zone of the porphyry deposit upward to the propylitic halo (e.g.,

* Corresponding author at: Departamento de Geología y Petróleo, Facultad de Ingeniería, Universidad Nacional del Comahue, Buenos Aires 1400, 8300 Neuquén, Argentina.
E-mail address: lauramaydagan@yahoo.com.ar (L. Maydagán).

https://doi.org/10.1016/j.oregeorev.2017.11.028
Received 10 August 2017; Received in revised form 20 November 2017; Accepted 27 November 2017
Available online 28 November 2017
0169-1368/

Cohen, 2011; Cooke et al., 2014; Wilkinson et al., 2015). However, there are few studies that document in detail the links between phyllosilicate geochemical variations and metals introduction in phyllic and propylitic halos of shallow porphyry enviroments.

In this paper we present the variations in the chemical composition of white micas and chlorites together with the distribution of clays and metals in the shallow propylitic and phyllic halos of the Quebrada de la Mina (QDM) Cu-Au porphyry deposit, San Juan Province (Argentina). Our results indicate that the geochemical variations of chlorites and white micas are indicative of the proximity to the channels of hydrothermal fluids linked to metals precipitation, and have the potential to be used as a guide for exploration in porphyry deposits.

QDM project has been recently acquired by Sibanye Gold Limited, subsidiary company of Peregrine Argentina S.A, which is conducting an environmental baseline study and preliminary economic evaluations for a copper-gold mining project.

2. Tectonic and geological setting

The QDM project (31°29′S, 70°30′W) is located in the SW of San Juan Province (Argentina), in the Andean Main Cordillera over the flat-slab segment (27–33° S) of the Southern Central Andes (Cahill and Isacks, 1992; Anderson et al., 2007; Gans et al., 2011). In the study area, the oldest exposed rocks comprises a late Carboniferous tonalitic batholith dated at 297 Ma (Maydagán, 2012) and Cretaceous volcanic and sedimentary rocks present along the Argentinian-Chilean boundary (Mpodozis et al., 2009). The QDM district is hosted by early Miocene volcanic rocks (Maydagán et al., 2011) which are equivalent to the Abanico Formation in Chile (Klohn, 1960), the Pachón Formation in the vicinity of the Los Pelambres deposit, the Coya Machalí Formation in the El Teniente area (Charrier et al., 2002) and the Doña Ana Group of the El Indio belt (Kay and Mpodozis, 2002).

Early Miocene volcanic rocks are widespread at QDM (Fig. 1) and consist of intercalations of basaltic andesite lavas, porphyritic andesite lavas, and polymictic volcanic breccias that grade upwards to levels dominated by pyroclastic rocks. The volcanic sequence is deformed and on the western ridges shows a N−S trend and dips ~40° to the west (Maydagán et al., 2016b). Early Miocene volcanic rocks were intruded by a circular dacite porphyry stock approximately 0.6 km in diameter (QDM porphyry, Fig. 2) that crops out on the northern ridges of the prospect (Fig. 1). The QDM porphyry intrusion has an U-Pb zircon age of 11.91 ± 0.33 Ma (Maydagán et al., 2016b). QDM porphyry has phenocrysts of plagioclase (35–40 vol%, 0.1–7 mm), amphibole (5 vol %, 0.2–2 mm), biotite (1.5 vol%, 5 mm), and quartz (1.5–3 vol%, 0.2–2 mm) in a microgranular (0.01–0.02 mm) to cryptocrystalline groundmass. A polymictic matrix-supported breccia (Late Breccia) with a N−S trend intruded the volcanic sequence and the QDM porphyry (Fig. 1). It contains rounded fragments of volcanic rocks, porphyry, and breccias (up to 60 cm) in an aphanitic greenish matrix. Locally, monomictic clast-supported tourmaline-cemented breccias cut the volcanic rocks, the porphyry, and the matrix-supported breccia (Maydagán et al., 2016b).

3. Analytical techniques and sampling methodology

Thirty days were spent mapping in the field and 50 surface samples were selected. Field data were collected from examination of outcrops and approximately 2000 m of core from 10 drill holes were chosen from cross sections 6517700 mN, 6517600 mN, and 2355800 mE of the Quebrada de la Mina deposit. The samples were studied first with a binocular polarizing microscope. Polished thin sections of 41 samples corresponding to the different lithologies, alteration zones, mineralization, and veins were analyzed under transmitted and reflected light.

Representative samples of the different pulses of alteration and mineralization were selected for X-ray analysis (n = 20). Phyllosilicates were identified using a Rigaku DMAX-2D diffractometer at the Centro de Investigaciones en Minerales Arcillosos de la Universidad Nacional del Comahue, Neuquén. In each sample studied, the total fraction and the oriented aggregates < 2 μm were analyzed from 2° to 40° 2θ, at 2° 2θ/min using a Cu-Kα radiation and X-ray diffraction traces at 40 kV and 20 mA. The XRD reflections were evaluated with Rigaku software.

Whole-rock samples (each corresponding to half pieces of drill core approximately 8 cm long and 2 cm thick) were crushed and ground with a mortar and pestle and then 30 g of each powdered whole rock were dispersed in one liter of distilled water and dispersed by ultrasonic probe. The < 2 μm fraction was separated by timed centrifugation. Oriented preparations of Sr-saturated < 2 μm fraction were analyzed by means of X-ray diffraction (XRD) in air-dried (AD) state (drying at room conditions), ethylene glycol (EG) solvation, and heating to 375 °C and 550 °C for one hour. Semi-quantitative clay analyses were carried out using the NEWMOD© program (Reynolds and Reynolds, 1996) and the Mineral Intensity Factor (MIF) method described in Moore and Reynolds (1997).

The illite crystallinity index was determined by measuring the width of the 001 illite peak for the < 2 μm fraction measured in degrees 2θ at half-peak height, using the method of Kübler (1964, 1967), and following the recommendations of Kisch (1991) for sample preparation.

Mid-infrared (MIR) spectra (400–4000 cm^{-1}) of clay material were acquired on KBr pellets using a Nicolet 760 FT-IR spectrometer from the Universite' de Poitiersequipped with a potassium bromide (KBr) beam splitter and DTGSKBr detector. The resolution was set at 4 cm^{-1} with co-addition of 100 scans. KBr pellets contained 1 mg of sample for 150 mg of KBr powder, crushed into a mortar and pressed under 8 tons for 5 min in a hydraulic press before drying at 120 °C.

The chemical compositions of chlorite and white mica from 11 samples (polished thin sections) were collected using a CAMECA SX-100 electron microprobe (EPMA) at Oregon State University (Tables 1 and 2). Analyses were conducted using a 15 kV accelerating voltage, 30 nA beam current, and 5 μm beam diameter with counting times between 10 and 30 s. Raw data were corrected using a stoichiometric PAP correction model (Pouchou and Pichoir, 1984) to a suite of natural and synthetic standards by microprobe software, which also provides estimates of lower limit of detection for each element. In addition, high-resolution backscatter electron (BSE) images of minerals were acquired.

4. Hydrothermal alteration zones

Six alteration zones were defined from a detailed petrographic study of 40 samples based on the presence and relative abundance of alteration minerals. Fig. 1 shows the alteration halos at the surface along with the contour of the volcanic wall rocks, QDM porphyry and late breccia. Sections 6517600 mN, 6517700 mN, and 2355800 mE show the distribution of the lithologies, alteration zones, and the location of the samples analyzed in this study (Fig. 2). Hydrothermal alteration in the Quebrada de la Mina porphyry Cu-Au deposit consists of a large phyllic area surrounded by a propylitic zone. Inside the phyllic zone there are small relicts of potassic alteration (Fig. 2). In the following text, the minerals of the hydrothermal assemblages are listed and separated by the symbol (+) if they are in equal amounts and with (±) if the mineral is in minor quantity or is rarely present. A relict mineral is given in parentheses after the mineral that replaces it, and a mineral not necessarily contemporaneous with the assemblage is separated by commas.

Quartz + K-feldspar ± rutile (potassic alteration), white mica, fine-grained clay mixtures alteration is found as patches at intermediate levels, replacing phenocrysts of plagioclase and the groundmass of the porphyry and the volcanic wall-rocks (Figs. 2, 3A, B). The mineralization consists of chalcopyrite (0.5 vol%, 0.1–0.2 mm) and pyrite (0.5 vol %, 0.1–0.2 mm). White mica and clays are superimposed on the primary assemblage and replace phenocrysts and groundmass to variable degrees.

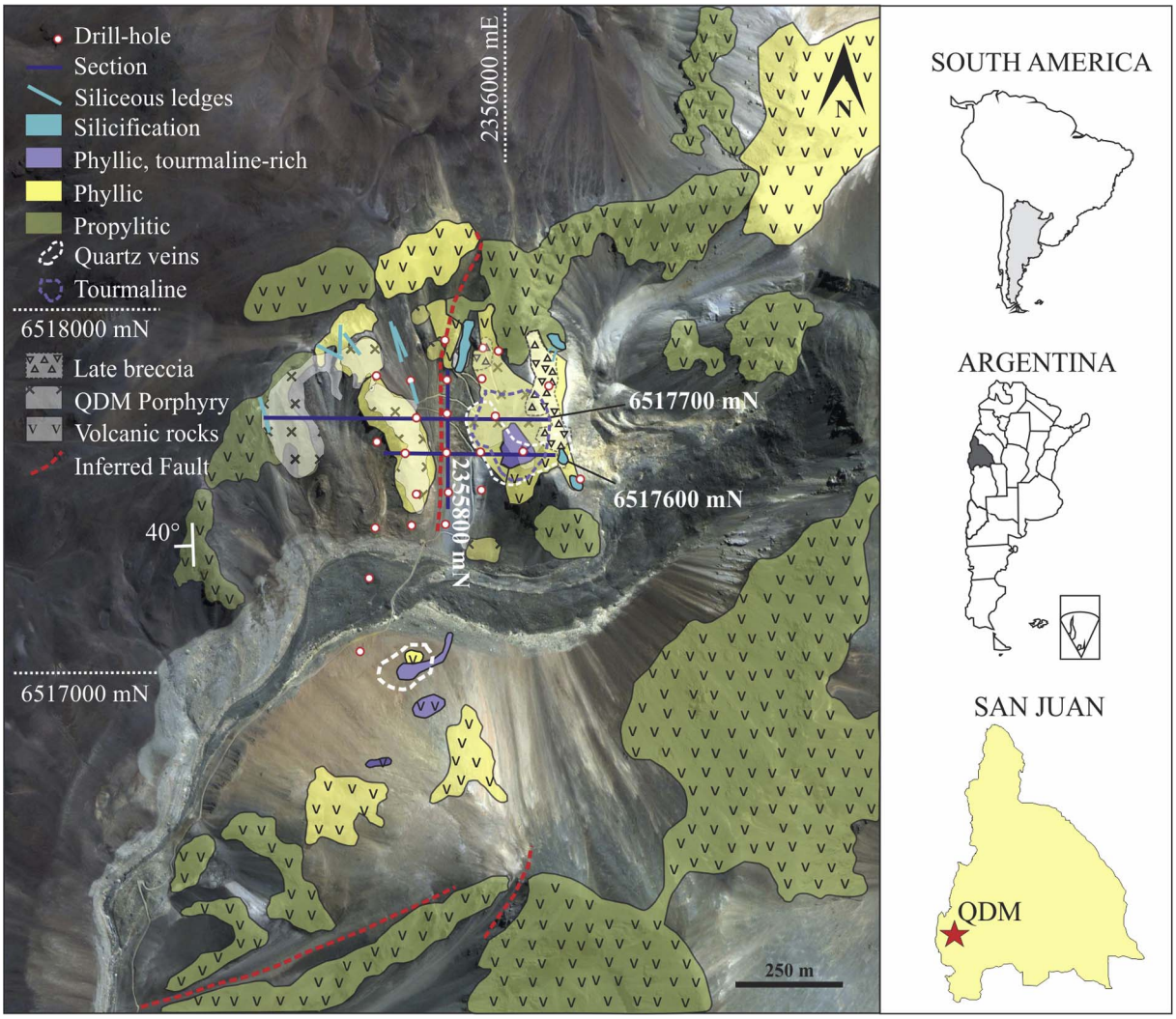

Fig. 1. Geologic map of QDM deposit (San Juan Province, Argentina) with the distribution of the hydrothermal alteration, quartz veins, drill-holes and location of W-E and N-S sections analyzed (Gauss Krueger coordinates, Inchauspe).

Chlorite ± epidote ± quartz ± rutile ± calcite (relict K-feldspar), white mica, fine-grained clay mixtures (propylitic alteration) occurs in the outer halo at the surface and at intermediate and shallow levels of the profiles affecting the wall rocks and the porphyry (Figs. 1, 2). Amphibole and biotite phenocrysts are replaced by chlorite ± rutile, whereas the groundmass is weakly altered to chlorite ± quartz (Fig. 3C). Plagioclase phenocrysts are partially dissolved and replaced by epidote ± calcite. This secondary assemblage usually contains hydrothermal K-feldspar as a relict mineral.

White mica + quartz ± tourmaline ± rutile ± anhydrite, fine-grained clay mixtures (phyllic alteration) affects the volcanic wall rocks, the porphyry, and late breccia. It is well developed in the center and uppermost part of the project where it forms a continuous halo that overprint the propylitic alteration (Figs. 1, 2, 3D–E). Locally, this assemblage completely obliterates the texture of the porphyry. The mineralization consists of two populations of pyrite crystals disseminated in the altered rocks: one as porous anhedral crystals (0.4–1 mm) and another one as very fine-grained anhedral crystals (0.01–0.3 mm). Locally, it contains anhedral sphalerite crystals associated with white mica, quartz, and pyrite (Fig. 3D).

Locally, tourmaline (15–20 vol%) replaces phenocrysts and groundmass of the rocks that acquire a dark color (Figs. 2, 3F). In these zones, with tourmaline rich-phyllic alteration (tourmaline + quartz + white mica ± barite, fine-grained clay mixtures) occur at the surface and at intermediate to shallow levels, overlapping earlier phyllic alteration zones (Figs. 2, 3F). Mineralization associated with this alteration consists of disseminated anhedral pyrite (3–5 vol%, 0.04–0.08 mm) and traces of tennantite, enargite, marcasite, and gold.

The western and central ridges of the project are affected by silicification grading into outer propylitic alteration zones. Siliceous ledges 2–3 m thick crop out at the surface (Figs. 1, 2) cutting the porphyry with a radial arrangement around the central valley of QDM.

Supergene alteration resulted in a leached cap characterized by jarosite + hematite veins and disseminations, and a weakly developed zone of sulfide enrichment (digenite ± covellite) of early sulfides. The leaching area has a thickness between 25 and 75 m (Fig. 2) and is poorly developed as jarosite and hematite are commonly accompanied by unoxidized pyrite.

4.1. Vein generations

The detailed study of QDM samples permitted the definition of five types of veins: A, M, C, D, and E veins (see Gustafson and Hunt, 1975; Gustafson and Quiroga, 1995; Masterman et al., 2005).

Fragments of veins composed mainly by anhedral quartz crystals associated with magnetite and traces of gold were recognized in the QDM-007 (A veins). Magnetite ± pyrite ± Au veinlets (M veins) are very scarce and cut the volcanic wall rocks affected by K-feldspar + quartz ± rutile and by phyllic alterations at intermediate depths of drill hole QDM-007 (Fig. 3A). These veins have straight walls

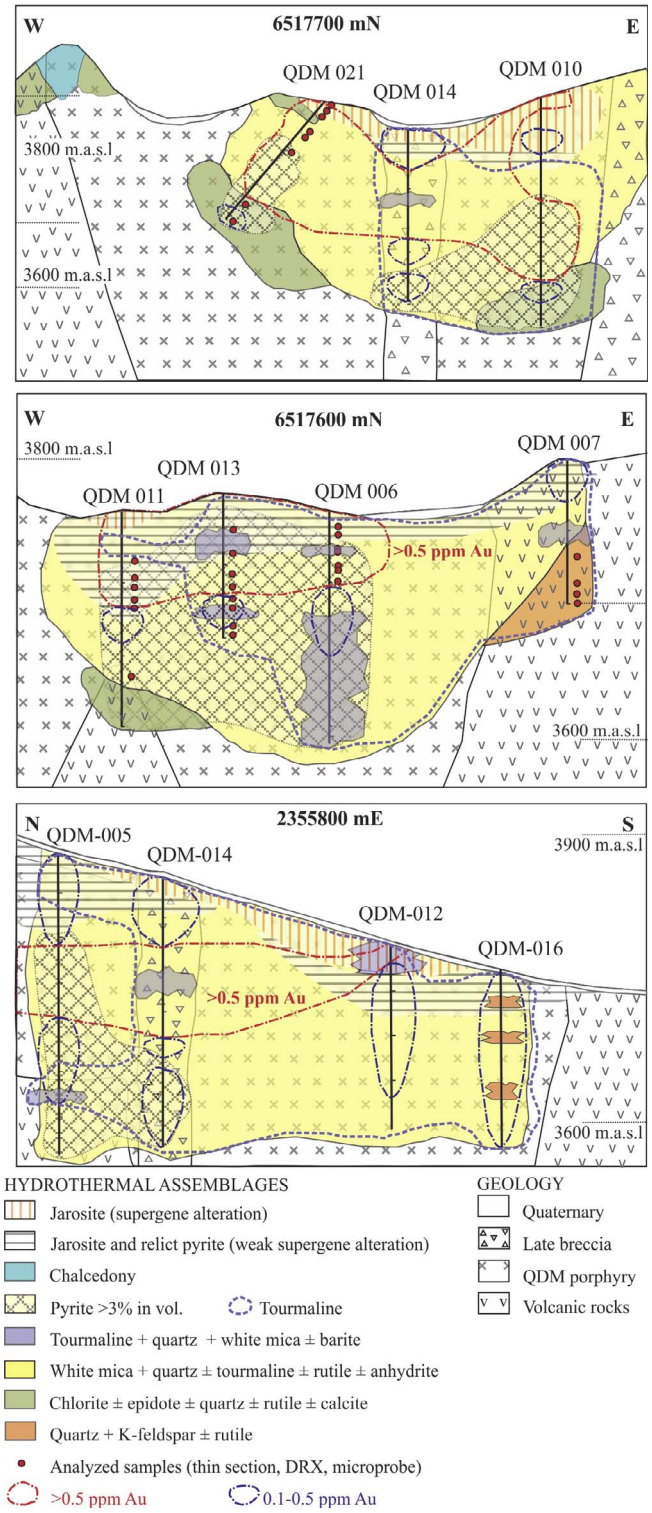

Fig. 2. W-E sections and N-S section analyzed with the distribution of lithologies, hydrothermal alteration types, Au-rich zones, and samples studied in thin section, X-ray diffraction, and electron microprobe.

and thicknesses ranging from ~2 mm to 4 cm. M veins are replaced by hematite veins (C veins) that cut the porphyry and the wall rocks with phyllic alteration at the surface. These veins are composed of hematite crystals (0.025–0.01 mm, after magnetite). They present straight walls and thicknesses up to 4 cm. On the eastern ridges that surround the district, epidote veins cut the volcanic wall-rocks with propylitic alteration.

D veins are characterized by phyllic alteration halos that range in width from 1 to 3 cm. They cut the porphyry and the volcanic wall rocks at the surface (Fig. 1) and at intermediate to shallow levels of the sections. Three subtypes of D veins were recognized: D1, D2, and D3. D1 veins consist of quartz + pyrite + chalcopyrite + sphalerite (Fig. 3B), have a thickness of 2 mm, and weak phyllic haloes (that partially preserve K-feldspar). They occur at intermediate levels of the volcanic wall rocks affected by K-feldspar + quartz ± rutile and by phyllic alterations (QDM-007). In the margins of these veins, anhedral and fine-grained quartz crystals were recognized. Towards the center of the vein, subhedral and coarse-grained euhedral quartz crystals show a perpendicular disposition to the vein walls, typical of D veins, and are in equilibrium with the sulfides that occupy the axial fracture.

D2 veins consist of pyrite ± white micas ± quartz (0.1–6 cm thick) and have straight walls (Fig. 3E). Subhedral pyrite (0.4–4 mm) crystals constitute 90% of the vein accompanied by mica and subhedral grains of quartz. In two samples, gold grains (10–20 μm) were recognized included in quartz of these veins cutting the QDM porphyry (QDM-021-58 m depth). D3 are irregular and thin (0.5–1 mm) veinlets composed of radial aggregates (1–3 mm) of acicular tourmaline with subordinate fine-grained (< 0.2 mm) quartz and pyrite crystals that cut the porphyry with phyllic alteration.

Late veins, veinlets, and stringers rich in sulfides and sulfosalts (type E) are composed of chalcopyrite, tennantite (chalcopyrite, bornite) ± gold, enargite (chalcopyrite, bornite, tennantite), marcasite and covellite. They are generally thin (0.5–1 mm), irregular, and discontinuous and cut D veins.

5. Metals distribution

Fig. 4 shows the distribution of metals in the N–S section 2355800 mE based on the geochemical analyses of the drill-holes performed by the exploration company. The highest values of Ag are located above ~3700–3750 m.a.s.l. (meters above the see level). High concentrations of Au occur in a subhorizontal zone between 3700 and 3800 m.a.s.l, that partially overlap the Ag-rich zone to the north. Zinc is concentrated in shallow levels of QDM-005 between 3750 and 3850 m.a.s.l, partially overlapping the Au-rich zone but extending to shallower levels. Values of Pb (> 150 ppm) occur in the northern part of the profile, above 3800 m.a.s.l. Values of As (< 0.05%) are present above 3800 m.a.s.l of drill holes QDM-005 and 014, and are also found in deep levels in the southern sector of the section. Small anomalies of Sb occur in deep levels of QDM-016, within the Au-rich zone cut by QDM-013, and in the upper sector of QDM-005. Anomalies of Cu overlap the arsenic values. Molybdenum is concentrated in the southern part of the section, below 3750 m.a.s.l, especially in drill holes QDM-012 and QDM-016. High values of Fe are located in deep levels of the northern sector of the section.

In the section 2355800 mN, the Au-rich zone occurs in the phyllic alteration halo and locally in tourmaline-rich zones, partially overlaps the upper levels of pyrite-rich zones, and at shallower levels partially overlaps zones with weak supergene alteration (with pyrite and jarosite). Au decreases in zones with potassic and propylitic alteration assemblages. Silver and Zn anomalies occur in zones of phyllic alteration, distal to the potassic patches. Arsenic contents are present in shallow levels and in deep levels close to the zones with relicts of potassic alteration where there are associated with antimony anomalies. Iron values coincide with pyrite-rich zones in phyllic and tourmaline-rich phyllic alterations. Copper and Mo are concentrated at deep levels around the transitional potassic- phyllic alterations in QDM-012 and QDM-016 (Fig. 4).

Gold shows moderate positive correlation (Pearson Product correlation coefficient, r) with Ag (r = 0.53, r = 0.60) in the 6517700 mN and 6517600 mN sections and weak positive correlation with Ag (r = 0.33) in the 2355800 mN section (Table 3). In the three sections analyzed, Au exhibits a weak positive correlation with Fe

Table 1
Representative microprobe analyses of hydrothermal clinochlore from the different alteration zones in the Quebrada de la Mina deposit.

Sample n°	QDM 021	QDM 021	QDM 021	QDM 021	QDM 021	QDM 021	QDM 021	QDM 021	QDM 021	QDM 021	QDM 021	QDM 021	QDM 021	QDM 021	QDM 021	QDM 021
Depth (m)	243	243	243	243	243	243	243	243	243	243	211	211	211	211	211	211
M.a.s.l	3633	3633	3633	3633	3633	3633	3633	3633	3633	3633	3665	3665	3665	3665	3665	3665
Lithology	QDM porph.	QDM porph.	QDM porph.	QDM porph.	QDM porph.	QDM porph.	QDM porph.	QDM porph.	QDM porph.	QDM porph.	QDM porph.	QDM porph.	QDM porph.	QDM porph.	QDM porph.	QDM porph.
Alteration	Propylitic	Propylitic	Propylitic	Propylitic	Propylitic	Propylitic	Propylitic	Propylitic	Propylitic	Propylitic	Propylitic	Propylitic	Propylitic	Propylitic	Propylitic	Propylitic
SiO_2	27.58	27.52	27.42	27.28	28.66	27.71	28.12	28.43	27.99	27.40	28.26	27.97	29.99	28.76	27.99	29.75
TiO_2	0.05	0.03	0.03	0.05	0.05	0.07	0.04	0.04	0.07	0.04	0.06	0.04	0.04	0.04	0.06	0.07
Al_2O_3	21.02	21.06	21.00	20.64	22.71	21.20	20.40	20.45	20.13	20.69	20.50	20.63	22.00	20.72	20.63	21.74
FeO	20.24	20.90	20.51	20.68	21.38	20.29	18.99	20.29	19.68	20.62	19.84	19.12	17.29	17.56	19.18	15.64
MnO	1.06	1.00	1.00	0.96	1.10	1.15	1.03	1.17	1.16	1.07	1.43	1.40	1.36	1.44	1.40	1.09
MgO	17.59	17.00	16.80	17.06	13.85	16.23	18.29	17.35	18.16	17.61	17.74	16.60	15.18	17.42	15.83	14.10
CaO	0.05	0.04	0.08	0.06	0.03	0.07	0.07	0.06	0.07	0.11	0.06	0.28	0.07	0.07	0.03	0.06
Na_2O	0.05	0.02	0.03	0.04	0.03	0.01	0.01	0.02	0.01	0.04	0.02	0.03	0.02	0.02	0.04	0.03
K_2O	0.01	0.01	0.02	0.03	0.58	0.11	0.00	0.01	0.00	0.03	0.02	0.18	0.07	0.05	0.33	0.26
F	0.06	0.06	0.01	0.02	0.16	0.12	0.03	0.00	0.19	0.05	0.07	0.14	0.07	0.06	0.00	0.02
Cl	0.01	0.00	0.01	0.00	0.00	0.01	0.01	0.01	0.01	0.02	0.01	0.01	0.02	0.03	0.01	0.03
SO_2	0.05	0.03	0.02	0.03	0.00	0.01	0.05	0.04	0.03	0.05	0.04	0.05	0.05	0.06	0.05	0.02
P_2O_5	0.01	0.05	0.12	0.03	0.02	0.05	0.10	0.05	0.08	0.06	0.00	0.15	0.00	0.00	0.00	0.01
SrO	0.00	0.01	0.00	0.08	0.04	0.00	0.00	0.06	0.06	0.00	0.04	0.00	0.00	0.00	0.02	0.00
V_2O_3	0.07	0.16	0.17	0.08	0.09	0.09	0.05	0.00	0.22	0.21	0.16	0.11	0.02	0.04	0.08	0.04
Total	87.84	87.89	87.22	87.06	88.71	87.11	87.19	87.98	87.85	87.99	88.24	86.73	86.18	86.27	85.65	82.86
Reformatted oxide percentages based on 28 oxygens (with Fe^{2+}/Fe^{3+} and OH calculated assuming full site occupancy)																
Si	5.62	5.63	5.65	5.64	5.75	5.68	5.74	5.78	5.70	5.61	5.73	5.75	6.01	5.85	5.81	6.13
^{IV}Al	2.38	2.37	2.35	2.36	2.25	2.32	2.26	2.22	2.30	2.39	2.27	2.25	1.99	2.15	2.19	1.87
^{VI}Al	2.70	2.74	2.78	2.69	3.19	2.84	2.67	2.71	2.57	2.63	2.66	2.79	3.29	2.86	2.90	3.51
Ti	0.01	0.00	0.00	0.01	0.01	0.01	0.01	0.01	0.01	0.01	0.01	0.01	0.01	0.01	0.01	0.01
Fe^{2+}	3.45	3.58	3.53	3.58	3.59	3.48	3.24	3.45	3.35	3.53	3.36	3.29	2.90	2.99	3.33	2.70
Mn	0.18	0.17	0.17	0.17	0.19	0.20	0.18	0.20	0.20	0.18	0.25	0.24	0.23	0.25	0.25	0.19
Mg	5.35	5.19	5.16	5.26	4.14	4.96	5.56	5.26	5.51	5.38	5.36	5.08	4.54	5.28	4.90	4.33
Σ Oct.	11.69	11.68	11.65	11.71	11.11	11.49	11.66	11.62	11.64	11.74	11.64	11.41	10.96	11.38	11.38	10.74
Ca	0.01	0.01	0.02	0.01	0.01	0.01	0.01	0.01	0.02	0.03	0.01	0.06	0.01	0.02	0.01	0.01
Na	0.04	0.02	0.03	0.03	0.02	0.01	0.01	0.02	0.01	0.03	0.02	0.02	0.01	0.02	0.03	0.02
K	0.00	0.01	0.01	0.01	0.29	0.06	0.00	0.00	0.00	0.01	0.01	0.09	0.04	0.02	0.17	0.14
Σ Interlayer	0.05	0.03	0.05	0.06	0.32	0.08	0.02	0.03	0.03	0.07	0.04	0.18	0.06	0.06	0.21	0.18
F	0.08	0.07	0.02	0.03	0.20	0.16	0.04	0.00	0.24	0.06	0.09	0.18	0.09	0.07	0.00	0.02
Cl	0.00	0.00	0.01	0.00	0.00	0.00	0.01	0.01	0.01	0.01	0.00	0.01	0.02	0.02	0.01	0.02
Fe/(Fe + Mg)	0.39	0.41	0.41	0.40	0.46	0.41	0.37	0.40	0.38	0.40	0.39	0.39	0.39	0.36	0.40	0.38
^{1}T (°C)	321	319	316	318	301	312	302	295	308	322	304	301	258	285	291	239

All iron as Fe^{2+} (Foster, 1962). 1. Based on Cathelineau (1988) T (°C) = −61.92 + 321 * 98(IVAl). Porph.: porphyry; M.a.s.l: meters above sea level
U_2O_3 was below 0.01 in all analyses.

Table 2
Representative microprobe analyses of white mica from the different alteration zones in the QDM porphyry deposit.

Drill hole	QDM 021	QDM 021	QDM 007	QDM 007	QDM 007	QDM 007	QDM 007	QDM 021	QDM 021
Depth (m)	200	243	135	135	135	135	135	21	21
M.a.s.l	3676	3633	3746	3746	3746	3746	3746	3855	3855
Alteration (wt%)	Prop	Prop	Potassic	Potassic	Potassic	Potassic	Potassic	Phyllic	Phyllic
SiO_2	49.99	47.24	47.13	47.46	47.03	47.63	46.61	48.19	48.30
TiO_2	0.01	0.11	0.11	0.14	0.16	0.19	0.10	0.09	0.06
Al_2O_3	34.45	30.25	31.42	30.35	30.43	30.65	31.95	32.82	31.24
FeO	1.06	4.40	3.13	3.53	3.68	3.71	2.78	2.19	3.22
MnO	0.08	0.18	0.03	0.02	0.00	0.01	0.00	0.12	0.17
MgO	0.99	2.72	2.56	2.71	3.54	3.02	2.80	1.35	1.44
CaO	0.06	0.07	0.08	0.02	0.03	0.02	0.02	0.00	0.00
Na_2O	0.11	0.08	0.15	0.12	0.15	0.15	0.17	0.23	0.14
K_2O	10.30	9.20	8.77	9.50	9.32	9.82	9.25	10.51	10.56
SrO	0.00	0.02	0.02	0.01	0.00	0.09	0.03	0.00	0.00
F	0.00	0.23	0.20	0.28	0.38	0.23	0.19	0.02	0.07
Cl	0.01	0.00	0.03	0.01	0.04	0.02	0.02	0.00	0.00
SO_2	0.06	0.01	0.09	0.07	0.09	0.09	0.09	0.13	0.03
P_2O5	0.00	0.00	0.03	0.04	0.02	0.02	0.00	0.00	0.00
V_2O_3	0.00	0.03	0.00	0.08	0.00	0.12	0.00	0.10	0.00
Total	97.11	94.55	93.74	94.35	94.85	95.77	94.03	95.74	95.22
Structural formulae based on 11 oxygen atoms									
Si	3.23	3.21	3.18	3.20	3.16	3.18	3.14	3.21	3.14
^{IV}Al	0.77	0.82	0.82	0.80	0.84	0.82	0.86	0.79	0.86
^{IV}Al	1.86	1.57	1.67	1.62	1.57	1.59	1.68	1.79	1.53
Ti	0.00	0.01	0.01	0.01	0.01	0.01	0.01	0.00	0.00
Fe	0.10	0.22	0.16	0.18	0.19	0.19	0.14	0.11	0.16
Mn	0.00	0.00	0.00	0.00	0.00	0.00	0.00	0.01	0.01
Mg	0.06	0.27	0.26	0.27	0.35	0.30	0.28	0.13	0.14
Σ Oct.	2.02	2.08	2.10	2.08	2.12	2.09	2.11	2.01	1.84
Ca	0.00	0.01	0.01	0.00	0.00	0.00	0.00	0.00	0.00
Na	0.01	0.01	0.02	0.02	0.02	0.02	0.02	0.03	0.02
K	0.85	0.80	0.76	0.82	0.80	0.84	0.80	0.89	0.88
Σ Interlayer	0.87	0.81	0.79	0.84	0.82	0.86	0.82	0.94	0.90
F	0.00	0.05	0.04	0.06	0.08	0.05	0.04	0.00	0.01
Cl	0.00	0.00	0.00	0.00	0.00	0.00	0.00	0.00	0.00
Fe + Mg + Mn	0.16	0.49	0.42	0.45	0.54	0.49	0.42	0.25	0.31
Total Al	2.63	2.39	2.50	2.41	2.41	2.41	2.54	2.58	2.39
QDM 021	QDM 021	QDM 021	QDM 021	QDM 021	QDM 021	QDM 021	QDM 021	QDM 006	QDM 006
21	21	21	21	21	21	21	21	52	52
3855	3855	3855	3855	3855	3855	3855	3855	3766	3766
Phyllic	Phyllic	Phyllic	Phyllic	Phyllic	Phyllic	Phyllic	Phyllic	Phyllic	Phyllic
48.88	48.72	48.02	48.44	48.01	48.38	48.99	51.96	46.32	46.03
0.07	0.08	0.08	0.07	0.08	0.09	0.05	0.02	0.45	0.54
31.57	32.04	32.00	32.89	32.55	31.71	32.30	32.02	33.40	34.95
2.74	2.33	2.81	2.38	2.69	3.02	2.08	0.74	2.56	1.92
0.17	0.17	0.10	0.10	0.14	0.12	0.15	0.04	0.02	0.02
1.40	1.41	1.26	1.14	1.27	1.42	1.45	1.87	1.29	0.46
0.00	0.00	0.00	0.00	0.00	0.00	0.00	0.02	0.03	0.00
0.17	0.16	0.26	0.34	0.27	0.15	0.20	0.08	0.56	0.54
10.30	10.40	10.51	10.55	9.94	10.45	10.22	9.25	10.26	10.67
0.00	0.00	0.00	0.00	0.04	0.00	0.00	0.00	0.02	0.00
0.00	0.07	0.00	0.06	0.12	0.10	0.07	0.00	0.13	0.13
0.00	0.01	0.01	0.00	0.02	0.00	0.01	0.00	0.01	0.00
0.04	0.03	0.05	0.07	0.06	0.04	0.09	0.07	0.03	0.01
0.00	0.00	0.00	0.00	0.02	0.00	0.00	0.02	0.05	0.12
0.00	0.09	0.04	0.17	0.00	0.02	0.00	0.00	0.00	0.03
95.34	95.51	95.14	96.20	95.20	95.51	95.61	96.08	95.13	95.42
3.24	3.23	3.20	3.20	3.19	3.22	3.24	3.36	3.10	3.07
0.76	0.77	0.80	0.80	0.81	0.78	0.76	0.64	0.90	0.93
1.71	1.74	1.72	1.76	1.75	1.70	1.75	1.80	1.74	1.82
0.00	0.00	0.00	0.00	0.00	0.00	0.00	0.00	0.02	0.03
0.14	0.12	0.14	0.12	0.13	0.15	0.10	0.04	0.13	0.10
0.01	0.01	0.01	0.01	0.01	0.01	0.01	0.00	0.00	0.00
0.14	0.14	0.13	0.11	0.13	0.14	0.14	0.18	0.13	0.05
2.00	2.00	2.00	2.00	2.02	2.01	2.01	2.02	2.02	1.99
0.00	0.00	0.00	0.00	0.00	0.00	0.00	0.00	0.00	0.00
0.02	0.02	0.03	0.04	0.04	0.02	0.03	0.01	0.07	0.07
0.87	0.88	0.89	0.89	0.84	0.89	0.86	0.76	0.88	0.91
0.89	0.90	0.93	0.93	0.88	0.91	0.89	0.77	0.95	0.98
0.00	0.01	0.00	0.01	0.03	0.02	0.01	0.00	0.03	0.03

(*continued on next page*)

Table 2 (*continued*)

Drill hole	QDM 021	QDM 021	QDM 007	QDM 007	QDM 007	QDM 007	QDM 007	QDM 021	QDM 021		
Depth (m)	200	243	135	135	135	135	135	21	21		
M.a.s.l	3676	3633	3746	3746	3746	3746	3746	3855	3855		
Alteration (wt%)	Prop	Prop	Potassic	Potassic	Potassic	Potassic	Potassic	Phyllic	Phyllic		
0.00	0.00	0.00	0.00	0.00	0.00	0.00	0.00	0.00	0.00		
0.28	0.27	0.28	0.24	0.27	0.30	0.25	0.22	0.26	0.15		
2.47	2.51	2.52	2.56	2.56	2.48	2.51	2.44	2.64	2.75		
QDM 006	QDM 006	QDM 006	QDM 006	QDM 006	QDM 006	QDM 021	QDM 013	QDM 013	QDM 013	QDM 013	QDM 013
52	52	52	52	52	52	51	113	113	113	113	113
3766	3766	3766	3766	3766	3766	3825	3722	3722	3722	3722	3722
Phyllic	Phyllic	Phyllic	Phyllic	Phyllic	Phyllic	Phyllic	Phyllic	Phyllic	Phyllic	Phyllic	Phyllic
45.98	46.68	46.81	48.58	49.38	47.15	47.98	48.32	47.80	48.44	47.68	47.81
0.31	0.33	0.29	0.05	0.04	0.09	0.06	0.01	0.00	0.00	0.00	0.02
33.80	33.28	34.13	32.42	33.10	32.60	32.88	33.45	33.41	32.01	33.21	33.29
1.90	2.33	2.20	1.88	0.84	2.52	1.78	0.85	0.85	2.01	0.98	0.91
0.00	0.01	0.00	0.08	0.22	0.15	0.16	0.02	0.03	0.03	0.01	0.02
0.69	0.84	0.80	1.46	1.79	1.73	1.61	2.56	2.28	2.50	2.63	2.38
0.03	0.01	0.01	0.03	0.01	0.01	0.03	0.00	0.02	0.02	0.00	0.00
0.51	0.41	0.52	0.21	0.11	0.29	0.23	0.37	0.36	0.22	0.42	0.37
10.05	10.20	10.11	10.49	10.73	10.55	10.44	9.88	9.76	9.95	9.87	9.50
0.00	0.07	0.00	0.02	0.05	0.00	0.01	0.01	0.00	0.00	0.04	0.00
0.21	0.12	0.00	0.09	0.00	0.06	0.08	0.03	0.00	0.07	0.12	0.06
0.02	0.02	0.01	0.01	0.01	0.02	0.01	0.00	0.01	0.01	0.01	0.01
0.05	0.02	0.02	0.00	0.02	0.02	0.04	0.04	0.07	0.05	0.03	0.05
0.07	0.08	0.07	0.00	0.00	0.00	0.02	0.13	0.13	0.26	0.11	0.12
0.07	0.08	0.00	0.00	0.03	0.02	0.01	0.00	0.00	0.04	0.00	0.01
93.69	94.48	94.99	95.33	96.31	95.23	95.34	95.67	94.73	95.60	95.10	94.55
3.12	3.14	3.12	3.22	3.23	3.15	3.19	3.18	3.17	3.21	3.16	3.18
0.88	0.86	0.88	0.78	0.77	0.85	0.81	0.82	0.83	0.79	0.84	0.82
1.82	1.78	1.80	1.76	1.78	1.72	1.76	1.77	1.79	1.71	1.76	1.79
0.02	0.02	0.01	0.00	0.00	0.00	0.00	0.00	0.00	0.00	0.00	0.00
0.10	0.12	0.11	0.09	0.04	0.13	0.09	0.04	0.04	0.10	0.05	0.05
0.00	0.00	0.00	0.00	0.01	0.01	0.01	0.00	0.00	0.00	0.00	0.00
0.07	0.08	0.08	0.14	0.17	0.17	0.16	0.25	0.23	0.25	0.26	0.24
2.00	2.00	2.01	2.00	2.01	2.03	2.02	2.07	2.02	1.96	2.02	2.02
0.00	0.00	0.00	0.00	0.00	0.00	0.00	0.00	0.00	0.00	0.00	0.00
0.07	0.05	0.07	0.03	0.01	0.04	0.03	0.05	0.05	0.03	0.05	0.05
0.87	0.88	0.86	0.89	0.90	0.90	0.88	0.83	0.83	0.84	0.84	0.81
0.94	0.93	0.93	0.92	0.91	0.94	0.92	0.88	0.88	0.87	0.89	0.85
0.05	0.03	0.00	0.02	0.00	0.01	0.02	0.01	0.00	0.01	0.03	0.01
0.00	0.00	0.00	0.00	0.00	0.00	0.00	0.00	0.00	0.00	0.00	0.00
0.17	0.20	0.19	0.23	0.22	0.31	0.26	0.29	0.27	0.35	0.31	0.28
2.70	2.64	2.68	2.54	2.55	2.57	2.57	2.59	2.61	2.50	2.60	2.61
QDM 013	QDM 013	QDM 013	QDM 013	QDM 013	QDM 013	QDM 013	QDM 021	QDM 021	QDM 021	QDM 021	
113	113	113	113	113	113	113	29	29	29	29	
3722	3722	3722	3722	3722	3722	3722	3847	3847	3847	3847	
Phyllic	Phyllic	Phyllic	Phyllic	Phyllic	Phyllic	Phyllic	Phyllic	Phyllic	Phyllic	Phyllic	
45.02	49.10	47.53	49.03	48.58	47.55	48.06	48.82	47.95	48.53	48.54	
0.04	0.00	0.00	0.05	0.09	0.09	0.18	0.09	0.08	0.05	0.08	
31.35	32.13	32.30	34.58	32.71	32.06	31.83	33.22	32.71	34.26	32.48	
0.85	1.91	2.08	1.07	2.48	2.91	4.08	2.85	2.91	1.86	3.19	
0.02	0.00	0.00	0.02	0.05	0.03	0.05	0.09	0.07	0.03	0.08	
1.99	2.48	2.07	2.35	1.18	1.26	1.33	0.77	0.72	0.97	0.81	
0.00	0.00	0.00	0.04	0.01	0.00	0.01	0.02	0.01	0.00	0.01	
0.38	0.18	0.22	0.37	0.43	0.45	0.17	0.20	0.22	0.27	0.20	
8.03	9.64	9.86	9.87	9.74	10.39	8.73	9.98	9.98	10.24	10.23	
0.00	0.00	0.00	0.00	0.00	0.01	0.01	0.00	0.00	0.00	0.00	
0.00	0.08	0.02	0.04	0.00	0.00	0.00	0.02	0.00	0.00	0.10	
0.02	0.01	0.01	0.02	0.01	0.00	0.01	0.01	0.01	0.02	0.01	
0.38	0.01	0.10	0.06	0.00	0.03	0.02	0.02	0.01	0.01	0.03	
0.10	0.09	0.29	0.13	0.00	0.02	0.00	0.02	0.00	0.03	0.03	
0.03	0.01	0.00	0.00	0.02	0.00	0.07	0.00	0.01	0.07	0.06	
88.21	95.64	94.49	97.62	95.29	94.80	94.57	96.13	94.66	96.34	95.85	
3.20	3.23	3.19	3.22	3.21	3.19	3.20	3.21	3.19	3.18	3.21	
0.80	0.77	0.81	0.78	0.79	0.81	0.80	0.79	0.81	0.82	0.79	
1.82	1.72	1.74	1.89	1.76	1.72	1.70	1.78	1.76	1.82	1.74	
0.00	0.00	0.00	0.00	0.00	0.00	0.01	0.00	0.00	0.00	0.00	
0.05	0.09	0.10	0.05	0.12	0.15	0.20	0.14	0.15	0.09	0.16	
0.00	0.00	0.00	0.00	0.00	0.00	0.00	0.01	0.00	0.00	0.00	
0.21	0.24	0.21	0.23	0.12	0.13	0.13	0.08	0.07	0.09	0.08	
2.03	2.06	2.05	2.17	2.01	2.00	2.05	2.00	1.98	2.01	1.99	
0.00	0.00	0.00	0.00	0.00	0.00	0.00	0.00	0.00	0.00	0.00	
0.05	0.02	0.03	0.05	0.05	0.06	0.02	0.03	0.03	0.03	0.03	
0.73	0.81	0.84	0.83	0.82	0.89	0.74	0.84	0.85	0.85	0.86	

(*continued on next page*)

Table 2 (*continued*)

Drill hole	QDM 021	QDM 021	QDM 007	QDM 007	QDM 007	QDM 007	QDM 007	QDM 021	QDM 021		
Depth (m)	200	243	135	135	135	135	135	21	21		
M.a.s.l	3676	3633	3746	3746	3746	3746	3746	3855	3855		
Alteration (wt%)	Prop	Prop	Potassic	Potassic	Potassic	Potassic	Potassic	Phyllic	Phyllic		
0.78	0.83	0.87	0.88	0.88	0.95	0.77	0.87	0.88	0.89	0.89	
0.00	0.02	0.00	0.01	0.00	0.00	0.00	0.00	0.00	0.00	0.02	
0.00	0.00	0.00	0.00	0.00	0.00	0.00	0.00	0.00	0.00	0.00	
0.26	0.34	0.31	0.28	0.24	0.27	0.34	0.22	0.22	0.19	0.24	
2.62	2.49	2.55	2.67	2.55	2.53	2.50	2.57	2.57	2.64	2.53	
QDM 021	QDM 021	QDM 021	QDM 021	QDM 021	QDM 021	QDM 021	QDM 021	QDM 021	QDM 021	QDM 021	QDM 021
29	29	29	29	29	29	29	29	29	29	29	29
3847	3847	3847	3847	3847	3847	3847	3847	3847	3847	3847	3847
Phyllic	Phyllic	Phyllic	Phyllic	Phyllic	Phyllic	Phyllic	Phyllic	Phyllic	Phyllic	Phyllic	Phyllic
47.87	48.40	48.57	48.72	48.44	48.08	48.30	48.06	46.92	47.17	47.35	47.39
0.08	0.08	0.07	0.08	0.05	0.11	0.06	0.05	0.04	0.03	0.08	0.07
32.63	33.06	33.26	33.13	32.84	31.99	33.50	33.33	33.02	33.26	32.34	32.06
2.12	1.91	1.70	1.52	3.12	2.92	1.54	1.85	1.66	1.59	3.00	3.01
0.15	0.14	0.05	0.03	0.09	0.14	0.07	0.05	0.05	0.04	0.06	0.08
1.19	1.24	1.06	1.05	0.90	0.63	1.00	0.92	0.97	0.97	0.80	0.84
0.02	0.01	0.00	0.00	0.01	0.00	0.00	0.05	0.04	0.01	0.00	0.04
0.16	0.18	0.20	0.19	0.22	0.15	0.23	0.23	0.25	0.24	0.26	0.27
10.30	10.55	10.26	10.25	10.27	10.21	10.24	9.85	10.15	9.85	9.91	9.92
0.00	0.00	0.04	0.00	0.02	0.00	0.01	0.00	0.00	0.00	0.00	0.00
0.06	0.04	0.09	0.06	0.00	0.18	0.03	0.00	0.01	0.01	0.00	0.04
0.01	0.01	0.00	0.00	0.01	0.01	0.01	0.02	0.01	0.02	0.02	0.01
0.01	0.01	0.05	0.01	0.02	0.00	0.01	0.05	0.09	0.08	0.03	0.04
0.03	0.02	0.00	0.00	0.01	0.00	0.00	0.00	0.00	0.01	0.00	0.04
0.06	0.00	0.07	0.00	0.02	0.03	0.00	0.02	0.04	0.00	0.00	0.00
94.70	95.65	95.43	95.05	96.03	94.44	95.01	94.47	93.25	93.28	93.84	93.82
3.20	3.20	3.21	3.22	3.20	3.23	3.20	3.20	3.18	3.18	3.19	3.20
0.80	0.80	0.79	0.78	0.80	0.77	0.80	0.80	0.82	0.82	0.81	0.80
1.77	1.78	1.80	1.81	1.75	1.76	1.82	1.82	1.81	1.83	1.76	1.75
0.00	0.00	0.00	0.00	0.00	0.01	0.00	0.00	0.00	0.00	0.00	0.00
0.11	0.09	0.08	0.08	0.15	0.15	0.08	0.09	0.08	0.08	0.15	0.15
0.01	0.01	0.00	0.00	0.00	0.01	0.00	0.00	0.00	0.00	0.00	0.00
0.12	0.12	0.10	0.10	0.09	0.06	0.10	0.09	0.10	0.10	0.08	0.08
2.01	2.00	2.00	2.00	2.00	1.98	2.00	2.01	2.00	2.01	2.00	2.00
0.00	0.00	0.00	0.00	0.00	0.00	0.00	0.00	0.00	0.00	0.00	0.00
0.02	0.02	0.03	0.02	0.03	0.02	0.03	0.03	0.03	0.03	0.03	0.03
0.88	0.89	0.87	0.87	0.86	0.87	0.87	0.84	0.88	0.85	0.85	0.85
0.90	0.91	0.89	0.89	0.90	0.89	0.90	0.87	0.92	0.88	0.89	0.90
0.01	0.01	0.02	0.01	0.00	0.04	0.01	0.00	0.00	0.00	0.00	0.01
0.00	0.00	0.00	0.00	0.00	0.00	0.00	0.00	0.00	0.00	0.00	0.00
0.23	0.23	0.19	0.18	0.25	0.22	0.18	0.19	0.19	0.18	0.24	0.24
2.57	2.58	2.59	2.59	2.55	2.53	2.62	2.62	2.64	2.65	2.57	2.55
QDM 021	QDM 021	QDM 021	QDM 021	QDM 021	QDM 021	QDM 021	QDM 021	QDM 021	QDM 021	QDM 021	QDM 021
29	29	29	29	29	29	29	29	29	29	29	29
3847	3847	3847	3847	3847	3847	3847	3847	3847	3847	3847	3847
Phyllic	Phyllic	Phyllic	Phyllic	Phyllic	Phyllic	Phyllic	Phyllic	Phyllic	Phyllic	Phyllic	Phyllic
47.29	45.17	46.84	47.20	46.41	46.27	46.60	47.12	46.87	48.36	48.51	48.30
0.06	0.08	0.08	0.08	0.10	0.12	0.03	0.01	0.03	0.06	0.08	0.04
32.16	31.33	31.59	32.25	31.42	30.54	33.00	32.42	32.11	33.98	33.50	32.01
3.13	3.08	3.03	3.37	3.54	3.23	2.17	2.61	3.23	1.64	1.63	3.14
0.09	0.07	0.12	0.13	0.13	0.13	0.06	0.12	0.10	0.07	0.06	0.13
0.88	0.98	0.89	0.93	1.12	1.20	0.74	0.94	0.85	0.83	0.95	1.01
0.03	0.06	0.02	0.03	0.03	0.03	0.01	0.01	0.03	0.05	0.04	0.04
0.24	0.17	0.23	0.18	0.15	0.14	0.24	0.21	0.23	0.22	0.24	0.23
10.23	9.49	10.03	10.13	10.26	10.57	9.74	9.88	9.73	9.27	9.71	10.05
0.01	0.00	0.05	0.00	0.00	0.00	0.00	0.00	0.04	0.03	0.00	0.07
0.06	0.10	0.04	0.05	0.02	0.07	0.02	0.00	0.00	0.00	0.00	0.05
0.03	0.02	0.02	0.01	0.01	0.01	0.01	0.01	0.02	0.01	0.02	0.01
0.01	0.02	0.06	0.00	0.02	0.07	0.04	0.01	0.08	0.06	0.02	0.03
0.05	0.04	0.00	0.01	0.04	0.04	0.00	0.00	0.03	0.01	0.03	0.01
0.04	0.05	0.02	0.00	0.06	0.00	0.01	0.00	0.07	0.00	0.04	0.03
94.31	90.66	93.03	94.36	93.32	92.41	92.67	93.35	93.41	94.59	94.83	95.16
3.19	3.16	3.20	3.18	3.17	3.20	3.17	3.19	3.18	3.19	3.20	3.19
0.81	0.84	0.80	0.82	0.83	0.80	0.83	0.81	0.82	0.81	0.80	0.81
1.74	1.75	1.74	1.73	1.70	1.69	1.82	1.77	1.75	1.84	1.80	1.69
0.00	0.00	0.00	0.00	0.01	0.01	0.00	0.00	0.00	0.00	0.00	0.00
0.16	0.16	0.16	0.17	0.18	0.17	0.11	0.13	0.17	0.08	0.08	0.16
0.01	0.00	0.01	0.01	0.01	0.01	0.00	0.01	0.01	0.00	0.00	0.01
0.09	0.10	0.09	0.09	0.11	0.12	0.07	0.09	0.09	0.08	0.09	0.10
2.00	2.02	2.00	2.01	2.01	1.99	2.01	2.01	2.01	2.01	1.98	1.95
0.00	0.00	0.00	0.00	0.00	0.00	0.00	0.00	0.00	0.00	0.00	0.00

(*continued on next page*)

Table 2 (*continued*)

Drill hole	QDM 021	QDM 021	QDM 007	QDM 007	QDM 007	QDM 007	QDM 007	QDM 021	QDM 021		
Depth (m)	200	243	135	135	135	135	135	21	21		
M.a.s.l	3676	3633	3746	3746	3746	3746	3746	3855	3855		
Alteration (wt%)	Prop	Prop	Potassic	Potassic	Potassic	Potassic	Potassic	Phyllic	Phyllic		
0.03	0.02	0.03	0.02	0.02	0.02	0.03	0.03	0.03	0.03	0.03	0.03
0.88	0.85	0.87	0.87	0.89	0.93	0.85	0.85	0.84	0.78	0.82	0.85
0.91	0.88	0.91	0.90	0.92	0.96	0.88	0.88	0.88	0.82	0.85	0.88
0.01	0.02	0.01	0.01	0.00	0.02	0.00	0.00	0.00	0.00	0.00	0.01
0.00	0.00	0.00	0.00	0.00	0.00	0.00	0.00	0.00	0.00	0.00	0.00
0.25	0.27	0.25	0.27	0.30	0.30	0.19	0.23	0.26	0.17	0.18	0.26
2.55	2.59	2.54	2.56	2.53	2.49	2.65	2.59	2.57	2.64	2.60	2.49
QDM 021	QDM 021	QDM 021	QDM 021	QDM 021	QDM 021	QDM 021	QDM 013	QDM 013	QDM 013	QDM 013	
29	29	29	29	29	51	51	113	154	154	154	
3847	3847	3847	3847	3847	3825	3825	3722	3681	3681	3681	
Phyllic	Phyllic	Phyllic	Phyllic	Phyllic	Phyllic	Phyllic	Phyllic	Tour Phyllic	Tour Phyllic	Tour Phyllic	
48.88	48.24	48.92	48.98	49.38	48.59	47.27	41.77	47.44	45.73	46.96	
0.07	0.05	0.04	0.02	0.05	0.06	0.06	0.06	0.13	0.18	0.14	
33.62	33.29	33.42	32.61	32.80	32.25	32.86	28.63	36.70	35.96	36.03	
1.72	1.49	2.28	2.56	2.42	1.41	2.61	0.82	0.36	0.48	0.80	
0.04	0.04	0.07	0.04	0.09	0.19	0.12	0.01	0.01	0.03	0.01	
0.84	0.94	0.60	0.60	0.70	1.57	1.04	1.94	0.37	0.34	0.54	
0.03	0.04	0.06	0.05	0.05	0.08	0.00	0.00	0.06	0.02	0.02	
0.28	0.29	0.28	0.27	0.24	0.16	0.19	0.33	0.66	0.71	0.61	
9.74	9.62	9.43	9.41	9.35	10.42	10.58	7.64	9.41	9.70	9.75	
0.00	0.01	0.02	0.00	0.00	0.03	0.00	0.00	0.00	0.04	0.00	
0.02	0.00	0.07	0.04	0.02	0.07	0.02	0.13	0.04	0.20	0.05	
0.01	0.01	0.01	0.00	0.01	0.01	0.00	0.08	0.01	0.01	0.01	
0.02	0.04	0.01	0.02	0.02	0.03	0.00	0.67	0.02	0.04	0.02	
0.00	0.01	0.02	0.01	0.00	0.04	0.00	0.11	0.37	0.24	0.12	
0.00	0.00	0.00	0.00	0.01	0.00	0.16	0.03	0.00	0.00	0.09	
95.29	94.07	95.25	94.62	95.15	94.89	94.93	82.22	95.59	93.70	95.15	
3.18	3.20	3.19	3.24	3.24	3.22	3.15	3.19	3.11	3.08	3.10	
0.82	0.80	0.81	0.76	0.76	0.78	0.85	0.81	0.89	0.92	0.90	
1.76	1.81	1.76	1.79	1.77	1.74	1.73	1.77	1.95	1.94	1.91	
0.00	0.00	0.00	0.00	0.00	0.00	0.00	0.00	0.01	0.01	0.01	
0.08	0.07	0.11	0.13	0.12	0.07	0.13	0.05	0.02	0.02	0.04	
0.00	0.00	0.00	0.00	0.01	0.01	0.01	0.00	0.00	0.00	0.00	
0.08	0.09	0.06	0.06	0.07	0.15	0.10	0.22	0.04	0.03	0.05	
1.93	1.98	1.94	1.98	1.97	1.98	1.98	2.05	2.01	2.01	2.01	
0.00	0.00	0.00	0.00	0.00	0.01	0.00	0.00	0.00	0.00	0.00	
0.03	0.04	0.04	0.03	0.03	0.02	0.03	0.05	0.08	0.09	0.08	
0.81	0.81	0.78	0.79	0.78	0.88	0.90	0.75	0.79	0.83	0.82	
0.85	0.86	0.83	0.84	0.82	0.91	0.92	0.80	0.88	0.93	0.90	
0.01	0.00	0.02	0.01	0.00	0.02	0.00	0.03	0.01	0.04	0.01	
0.00	0.00	0.00	0.00	0.00	0.00	0.00	0.01	0.00	0.00	0.00	
0.17	0.17	0.17	0.19	0.19	0.24	0.24	0.27	0.05	0.06	0.09	
2.58	2.61	2.57	2.54	2.54	2.52	2.58	2.58	2.84	2.86	2.81	
QDM 013	QDM 013	QDM 013	QDM 013	QDM 021	QDM 021	QDM 021	QDM 021	QDM 021	QDM 021	QDM 021	
154	154	154	154	58	58	58	58	58	58	58	
3681	3681	3681	3681	3818	3818	3818	3818	3818	3818	3818	
Tour Phyllic	Tour Phyllic	Tour Phyllic	Tour Phyllic	D vein	D vein	D vein	D vein	D vein	D vein	D vein	
46.90	47.10	45.28	44.48	47.44	47.43	47.16	47.75	46.98	47.48	47.93	
0.11	0.20	0.22	0.19	0.08	0.08	0.15	0.07	0.11	0.06	0.11	
36.62	33.51	31.56	34.15	32.98	33.05	33.84	32.57	31.99	33.17	31.84	
0.44	0.93	1.86	0.75	2.88	2.87	2.23	3.14	3.33	2.94	3.86	
0.02	0.00	0.02	0.02	0.08	0.09	0.08	0.09	0.13	0.07	0.14	
0.42	0.62	1.29	0.45	1.02	1.05	0.98	1.19	1.20	0.99	1.40	
0.03	0.07	0.04	0.02	0.04	0.00	0.02	0.02	0.02	0.00	0.01	
0.66	0.56	0.50	0.55	0.36	0.26	0.27	0.16	0.26	0.19	0.08	
9.71	9.29	10.03	8.89	10.08	10.54	10.27	10.45	10.28	10.45	11.03	
0.00	0.00	0.00	0.00	0.00	0.00	0.00	0.00	0.00	0.02	0.00	
0.08	0.12	0.18	0.05	0.20	0.00	0.01	0.00	0.07	0.02	0.23	
0.01	0.03	0.03	0.04	0.02	0.01	0.00	0.00	0.01	0.00	0.01	
0.03	0.06	0.06	0.09	0.06	0.02	0.04	0.05	0.05	0.03	0.00	
0.18	0.09	0.07	0.30	0.01	0.01	0.02	0.00	0.04	0.00	0.01	
0.00	0.05	0.03	0.03	0.00	0.05	0.04	0.02	0.02	0.00	0.06	
95.21	92.62	91.15	90.01	95.25	95.45	95.12	95.50	94.49	95.42	96.70	
3.09	3.19	3.16	3.11	3.16	3.16	3.14	3.17	3.17	3.16	3.18	
0.91	0.81	0.84	0.89	0.84	0.84	0.86	0.83	0.83	0.84	0.82	
1.94	1.87	1.75	1.92	1.76	1.75	1.79	1.73	1.71	1.76	1.66	
0.01	0.01	0.01	0.01	0.00	0.00	0.01	0.00	0.01	0.00	0.01	
0.02	0.05	0.10	0.04	0.14	0.14	0.11	0.16	0.17	0.15	0.19	
0.00	0.00	0.00	0.00	0.00	0.01	0.00	0.01	0.01	0.00	0.01	
0.04	0.06	0.13	0.05	0.10	0.10	0.10	0.12	0.12	0.10	0.14	

(*continued on next page*)

Table 2 (*continued*)

Drill hole	QDM 021	QDM 021	QDM 007	QDM 007	QDM 007	QDM 007	QDM 007	QDM 021	QDM 021		
Depth (m)	200	243	135	135	135	135	135	21	21		
M.a.s.l	3676	3633	3746	3746	3746	3746	3746	3855	3855		
Alteration (wt%)	Prop	Prop	Potassic	Potassic	Potassic	Potassic	Potassic	Phyllic	Phyllic		
2.01	1.99	2.00	2.02	2.01	2.01	2.02	2.01	2.01	2.01	2.01	
0.00	0.01	0.00	0.00	0.00	0.00	0.00	0.00	0.00	0.00	0.00	
0.08	0.07	0.07	0.07	0.05	0.03	0.03	0.02	0.03	0.02	0.01	
0.82	0.80	0.89	0.79	0.86	0.90	0.87	0.89	0.88	0.89	0.93	
0.91	0.89	0.97	0.87	0.91	0.93	0.91	0.91	0.92	0.91	0.94	
0.02	0.03	0.04	0.01	0.04	0.00	0.00	0.00	0.01	0.00	0.05	
0.00	0.00	0.00	0.00	0.00	0.00	0.00	0.00	0.00	0.00	0.00	
0.06	0.11	0.23	0.09	0.25	0.25	0.21	0.28	0.30	0.25	0.34	
2.85	2.68	2.60	2.81	2.59	2.59	2.65	2.55	2.54	2.60	2.49	
QDM 021	QDM 021	QDM 021	QDM 021	QDM 021	QDM 021	QDM 021	QDM 021	QDM 021	QDM 021	QDM 021	QDM 021
58	58	58	58	58	58	58	58	58	58	58	58
3818	3818	3818	3818	3818	3818	3818	3818	3818	3818	3818	3818
D vein	D vein	D vein	D vein	D vein	D vein	D vein	D vein	D vein	D vein	D vein	D vein
47.52	47.71	48.51	47.52	48.90	47.75	48.53	46.98	47.73	48.01	47.05	46.78
0.11	0.09	0.13	0.10	0.13	0.10	0.12	0.08	0.06	0.10	0.06	0.19
32.51	32.01	33.49	32.32	32.26	32.12	32.91	31.31	32.28	31.97	31.81	34.28
3.21	3.43	2.22	3.24	2.73	3.39	2.73	3.52	3.01	3.41	3.19	1.85
0.12	0.10	0.04	0.08	0.08	0.06	0.06	0.10	0.09	0.08	0.07	0.07
1.16	1.28	0.87	1.14	1.11	1.13	1.04	1.27	1.14	1.24	1.09	0.64
0.01	0.01	0.02	0.05	0.04	0.03	0.00	0.00	0.02	0.03	0.00	0.03
0.14	0.09	0.50	0.28	0.24	0.42	0.39	0.13	0.18	0.10	0.17	0.38
10.71	10.55	9.44	10.04	9.48	9.94	9.87	10.20	10.17	10.63	10.22	9.86
0.05	0.00	0.05	0.00	0.05	0.00	0.00	0.01	0.00	0.00	0.03	0.05
0.11	0.00	0.00	0.05	0.05	0.04	0.00	0.16	0.20	0.09	0.00	0.19
0.01	0.00	0.01	0.01	0.01	0.01	0.01	0.01	0.01	0.00	0.00	0.01
0.00	0.02	0.04	0.06	0.05	0.02	0.02	0.01	0.00	0.04	0.00	0.05
0.02	0.04	0.01	0.03	0.02	0.00	0.04	0.00	0.01	0.00	0.00	0.07
0.09	0.00	0.06	0.13	0.02	0.00	0.00	0.09	0.03	0.12	0.01	0.05
95.76	95.33	95.36	95.04	95.17	95.00	95.72	93.86	94.93	95.83	93.69	94.48
3.16	3.18	3.20	3.18	3.24	3.19	3.20	3.19	3.19	3.19	3.19	3.13
0.84	0.82	0.80	0.82	0.76	0.81	0.80	0.81	0.81	0.81	0.81	0.87
1.71	1.70	1.80	1.73	1.75	1.71	1.76	1.70	1.74	1.70	1.73	1.84
0.01	0.00	0.01	0.00	0.01	0.00	0.01	0.00	0.00	0.00	0.00	0.01
0.16	0.17	0.11	0.16	0.14	0.17	0.14	0.18	0.15	0.17	0.16	0.09
0.01	0.01	0.00	0.00	0.00	0.00	0.00	0.01	0.01	0.00	0.00	0.00
0.11	0.13	0.09	0.11	0.11	0.11	0.10	0.13	0.11	0.12	0.11	0.06
1.99	2.01	2.01	2.01	2.01	2.01	2.01	2.01	2.01	2.00	2.01	2.01
0.00	0.00	0.00	0.00	0.00	0.00	0.00	0.00	0.00	0.00	0.00	0.00
0.02	0.01	0.06	0.04	0.03	0.05	0.05	0.02	0.02	0.01	0.02	0.05
0.91	0.90	0.79	0.86	0.80	0.85	0.83	0.88	0.87	0.90	0.88	0.84
0.93	0.91	0.86	0.90	0.84	0.91	0.88	0.90	0.89	0.92	0.91	0.90
0.02	0.00	0.00	0.01	0.01	0.01	0.00	0.03	0.04	0.02	0.00	0.04
0.00	0.00	0.00	0.00	0.00	0.00	0.00	0.00	0.00	0.00	0.00	0.00
0.28	0.31	0.20	0.28	0.25	0.29	0.24	0.31	0.27	0.30	0.28	0.16
2.55	2.52	2.60	2.55	2.52	2.53	2.56	2.51	2.54	2.51	2.54	2.71
QDM 021	QDM 021	QDM 021	QDM 021	QDM 021	QDM 021	QDM 021	QDM 021	QDM 021	QDM 021	QDM 021	QDM 021
58	58	58	58	58	58	58	58	58	58	58	58
3818	3818	3818	3818	3818	3818	3818	3818	3818	3818	3818	3818
D vein	D vein	D vein	D vein	D vein	D vein	D vein	D vein	D vein	D vein	D vein	D vein
47.03	48.38	48.11	48.28	48.37	47.78	48.30	48.25	49.06	47.69	48.44	48.95
0.15	0.14	0.10	0.08	0.08	0.09	0.09	0.08	0.10	0.08	0.07	0.09
32.72	33.11	32.51	32.33	33.53	32.75	32.50	31.84	32.10	31.99	31.84	33.80
2.03	2.38	3.24	3.25	2.44	3.28	3.19	3.51	3.28	3.43	3.59	2.04
0.04	0.05	0.06	0.11	0.06	0.08	0.06	0.11	0.08	0.06	0.11	0.03
0.81	0.95	1.17	1.18	1.00	1.18	1.07	1.23	1.07	1.15	1.18	0.86
0.03	0.02	0.03	0.02	0.04	0.04	0.03	0.03	0.03	0.04	0.04	0.04
0.50	0.45	0.32	0.19	0.32	0.22	0.20	0.16	0.25	0.23	0.18	0.45
9.43	9.89	9.95	10.35	9.79	10.06	9.94	10.51	9.98	10.06	10.17	9.45
0.00	0.00	0.00	0.03	0.00	0.02	0.00	0.00	0.02	0.00	0.00	0.02
0.03	0.00	0.07	0.00	0.00	0.07	0.06	0.17	0.01	0.09	0.00	0.01
0.02	0.01	0.01	0.01	0.01	0.02	0.01	0.01	0.00	0.01	0.00	0.01
0.06	0.03	0.06	0.04	0.07	0.05	0.03	0.01	0.01	0.05	0.02	0.01
0.04	0.03	0.03	0.00	0.04	0.00	0.00	0.00	0.03	0.00	0.00	0.00
0.01	0.00	0.00	0.05	0.00	0.00	0.08	0.04	0.03	0.00	0.03	0.00
92.93	95.45	95.66	95.92	95.75	95.65	95.57	95.94	96.03	94.88	95.66	95.76
3.19	3.20	3.19	3.20	3.19	3.17	3.20	3.20	3.23	3.19	3.21	3.21
0.81	0.80	0.81	0.80	0.81	0.83	0.80	0.80	0.77	0.81	0.79	0.79
1.80	1.78	1.73	1.72	1.79	1.73	1.74	1.69	1.72	1.71	1.70	1.82
0.01	0.01	0.00	0.00	0.00	0.00	0.00	0.00	0.00	0.00	0.00	0.00
0.10	0.12	0.16	0.16	0.12	0.16	0.16	0.18	0.16	0.17	0.18	0.10

(*continued on next page*)

Table 2 (*continued*)

Drill hole	QDM 021	QDM 021	QDM 007	QDM 007	QDM 007	QDM 007	QDM 007	QDM 021	QDM 021		
Depth (m)	200	243	135	135	135	135	135	21	21		
M.a.s.l	3676	3633	3746	3746	3746	3746	3746	3855	3855		
Alteration (wt%)	Prop	Prop	Potassic	Potassic	Potassic	Potassic	Potassic	Phyllic	Phyllic		
0.00	0.00	0.00	0.01	0.00	0.00	0.00	0.01	0.00	0.00	0.01	0.00
0.08	0.09	0.12	0.12	0.10	0.12	0.11	0.12	0.10	0.11	0.12	0.08
2.00	2.00	2.01	2.01	2.01	2.02	2.01	2.00	2.00	2.01	2.01	2.01
0.00	0.00	0.00	0.00	0.00	0.00	0.00	0.00	0.00	0.00	0.00	0.00
0.07	0.06	0.04	0.02	0.04	0.03	0.03	0.02	0.03	0.03	0.02	0.06
0.82	0.83	0.84	0.87	0.82	0.85	0.84	0.89	0.84	0.86	0.86	0.79
0.89	0.89	0.89	0.90	0.87	0.89	0.87	0.91	0.87	0.89	0.89	0.85
0.01	0.00	0.02	0.00	0.00	0.02	0.01	0.04	0.00	0.02	0.00	0.00
0.00	0.00	0.00	0.00	0.00	0.00	0.00	0.00	0.00	0.00	0.00	0.00
0.19	0.22	0.28	0.28	0.22	0.29	0.27	0.30	0.27	0.29	0.30	0.19
2.62	2.58	2.54	2.52	2.60	2.56	2.54	2.49	2.49	2.52	2.49	2.61
QDM 021	QDM 021	QDM 021	QDM 021	QDM 021	QDM 021	QDM 021	QDM 021	QDM 021	QDM 021	QDM 021	QDM 021
58	58	58	58	58	58	58	58	58	58	58	58
3818	3818	3818	3818	3818	3818	3818	3818	3818	3818	3818	3818
D vein	D vein	D vein	D vein	D vein	D vein	D vein	D vein	D vein	D vein	D vein	D vein
45.61	48.67	45.87	48.00	49.26	47.70	47.87	47.91	47.77	48.31	47.83	46.45
0.15	0.07	0.13	0.07	0.09	0.09	0.09	0.10	0.11	0.09	0.11	0.14
35.75	32.14	33.22	31.88	32.54	32.55	32.42	32.01	32.30	32.79	31.97	30.80
0.83	3.13	1.69	3.31	3.15	3.05	3.25	3.46	3.23	2.50	3.47	3.82
0.05	0.10	0.09	0.10	0.09	0.10	0.07	0.13	0.11	0.12	0.15	0.11
0.39	1.20	0.73	1.23	1.12	1.09	1.10	1.26	1.19	1.03	1.33	1.30
0.01	0.02	0.00	0.00	0.02	0.02	0.02	0.02	0.05	0.04	0.02	0.01
0.55	0.19	0.35	0.12	0.28	0.20	0.19	0.16	0.11	0.20	0.10	0.16
9.79	10.33	9.68	10.74	9.74	10.46	10.03	10.45	10.48	10.18	10.34	9.97
0.01	0.00	0.00	0.06	0.00	0.00	0.01	0.05	0.04	0.00	0.01	0.00
0.13	0.22	0.00	0.06	0.08	0.02	0.00	0.07	0.00	0.07	0.04	0.09
0.03	0.01	0.04	0.01	0.01	0.01	0.00	0.01	0.01	0.01	0.00	0.02
0.10	0.01	0.06	0.02	0.06	0.04	0.03	0.02	0.03	0.03	0.01	0.09
0.09	0.03	0.07	0.03	0.04	0.01	0.04	0.11	0.02	0.03	0.00	0.01
0.02	0.05	0.03	0.02	0.00	0.00	0.04	0.03	0.06	0.03	0.00	0.07
93.51	96.18	91.98	95.64	96.49	95.32	95.16	95.80	95.51	95.41	95.38	93.05
3.07	3.20	3.12	3.16	3.21	3.14	3.18	3.17	3.17	3.19	3.18	3.16
0.93	0.80	0.88	0.84	0.79	0.86	0.82	0.83	0.83	0.81	0.82	0.84
1.91	1.69	1.79	1.64	1.71	1.67	1.72	1.67	1.69	1.74	1.68	1.63
0.01	0.00	0.01	0.00	0.00	0.00	0.00	0.00	0.01	0.00	0.01	0.01
0.04	0.16	0.09	0.16	0.15	0.15	0.16	0.17	0.16	0.12	0.17	0.20
0.00	0.01	0.01	0.01	0.01	0.01	0.00	0.01	0.01	0.01	0.01	0.01
0.04	0.12	0.07	0.12	0.11	0.11	0.11	0.12	0.12	0.10	0.13	0.13
2.00	1.98	1.96	1.93	1.99	1.94	2.00	1.98	1.98	1.98	2.00	1.97
0.00	0.00	0.00	0.00	0.00	0.00	0.00	0.00	0.00	0.00	0.00	0.00
0.07	0.02	0.05	0.02	0.04	0.03	0.02	0.02	0.01	0.03	0.01	0.02
0.84	0.87	0.84	0.90	0.81	0.88	0.85	0.88	0.89	0.86	0.88	0.86
0.91	0.89	0.89	0.92	0.85	0.91	0.88	0.91	0.91	0.89	0.89	0.89
0.03	0.05	0.00	0.01	0.02	0.00	0.00	0.01	0.00	0.01	0.01	0.02
0.00	0.00	0.00	0.00	0.00	0.00	0.00	0.00	0.00	0.00	0.00	0.00
0.08	0.28	0.17	0.29	0.27	0.26	0.28	0.30	0.29	0.23	0.31	0.33
2.84	2.49	2.67	2.48	2.50	2.53	2.54	2.50	2.52	2.55	2.50	2.47
QDM 021	QDM 021	QDM 021	QDM 021	QDM 021	QDM 021	QDM 006	QDM 006	QDM 006	QDM 006	QDM 006	QDM 006
58	58	58	58	58	58	98	98	98	98	98	98
3818	3818	3818	3818	3818	3818	3720	3720	3720	3720	3720	3720
D vein	D vein	D vein	D vein	D vein	D vein	D vein	D vein	D vein	D vein	D vein	D vein
47.90	48.08	48.52	47.59	47.82	46.05	49.03	48.27	47.64	48.34	47.95	48.37
0.11	0.11	0.08	0.12	0.09	0.08	0.05	0.04	0.04	0.08	0.16	0.19
32.17	32.19	31.98	32.14	32.22	33.19	33.08	32.98	32.07	33.11	33.71	33.73
3.35	3.36	3.26	3.24	3.32	1.70	2.70	2.61	2.11	2.26	1.94	2.16
0.13	0.11	0.12	0.09	0.12	0.03	0.02	0.01	0.03	0.00	0.01	0.01
1.32	1.26	1.31	1.19	1.15	0.71	1.12	1.12	1.61	1.14	0.91	0.99
0.05	0.03	0.00	0.00	0.02	0.04	0.03	0.05	0.05	0.01	0.01	0.02
0.17	0.19	0.12	0.27	0.14	0.42	0.54	0.54	0.46	0.52	0.54	0.47
10.33	10.33	10.57	10.20	10.29	9.13	9.86	10.08	10.26	10.16	9.99	10.20
0.00	0.00	0.00	0.01	0.00	0.00	0.03	0.00	0.03	0.02	0.00	0.00
0.00	0.08	0.00	0.13	0.02	0.16	0.33	0.37	0.41	0.41	0.32	0.27
0.01	0.00	0.01	0.01	0.01	0.03	0.01	0.01	0.02	0.01	0.01	0.01
0.01	0.03	0.00	0.00	0.03	0.37	0.01	0.01	0.03	0.00	0.00	0.03
0.04	0.06	0.00	0.01	0.07	0.03	0.00	0.03	0.04	0.00	0.00	0.00
0.01	0.04	0.00	0.05	0.00	0.12	0.00	0.00	0.00	0.06	0.01	0.00
95.60	95.85	95.97	95.06	95.30	92.06	96.82	96.12	94.78	96.11	95.58	96.44
3.17	3.18	3.19	3.16	3.18	3.15	3.19	3.16	3.16	3.18	3.14	3.17
0.83	0.82	0.81	0.84	0.82	0.85	0.81	0.84	0.84	0.82	0.86	0.83
1.68	1.70	1.66	1.68	1.71	1.83	1.73	1.71	1.67	1.75	1.74	1.77

(*continued on next page*)

Table 2 (*continued*)

Drill hole	QDM 021	QDM 021	QDM 007	QDM 007	QDM 007	QDM 007	QDM 007	QDM 021	QDM 021		
Depth (m)	200	243	135	135	135	135	135	21	21		
M.a.s.l	3676	3633	3746	3746	3746	3746	3746	3855	3855		
Alteration (wt%)	Prop	Prop	Potassic	Potassic	Potassic	Potassic	Potassic	Phyllic	Phyllic		
0.01	0.01	0.00	0.01	0.00	0.00	0.00	0.00	0.00	0.00	0.01	0.01
0.17	0.17	0.16	0.16	0.17	0.09	0.13	0.13	0.11	0.11	0.10	0.11
0.01	0.01	0.01	0.01	0.01	0.00	0.00	0.00	0.00	0.00	0.00	0.00
0.13	0.12	0.13	0.12	0.11	0.07	0.11	0.11	0.16	0.11	0.09	0.10
1.99	2.00	1.96	1.97	2.00	2.00	1.98	1.95	1.94	1.97	1.93	1.98
0.00	0.00	0.00	0.00	0.00	0.00	0.00	0.00	0.00	0.00	0.00	0.00
0.02	0.02	0.02	0.03	0.02	0.06	0.07	0.07	0.06	0.07	0.07	0.06
0.87	0.87	0.89	0.87	0.87	0.80	0.82	0.84	0.87	0.85	0.83	0.85
0.90	0.90	0.90	0.90	0.89	0.86	0.89	0.92	0.93	0.92	0.91	0.91
0.00	0.02	0.00	0.03	0.00	0.03	0.07	0.08	0.09	0.09	0.07	0.06
0.00	0.00	0.00	0.00	0.00	0.00	0.00	0.00	0.00	0.00	0.00	0.00
0.30	0.30	0.30	0.29	0.29	0.16	0.24	0.24	0.27	0.22	0.19	0.20
2.51	2.51	2.48	2.52	2.53	2.68	2.54	2.55	2.51	2.57	2.60	2.60

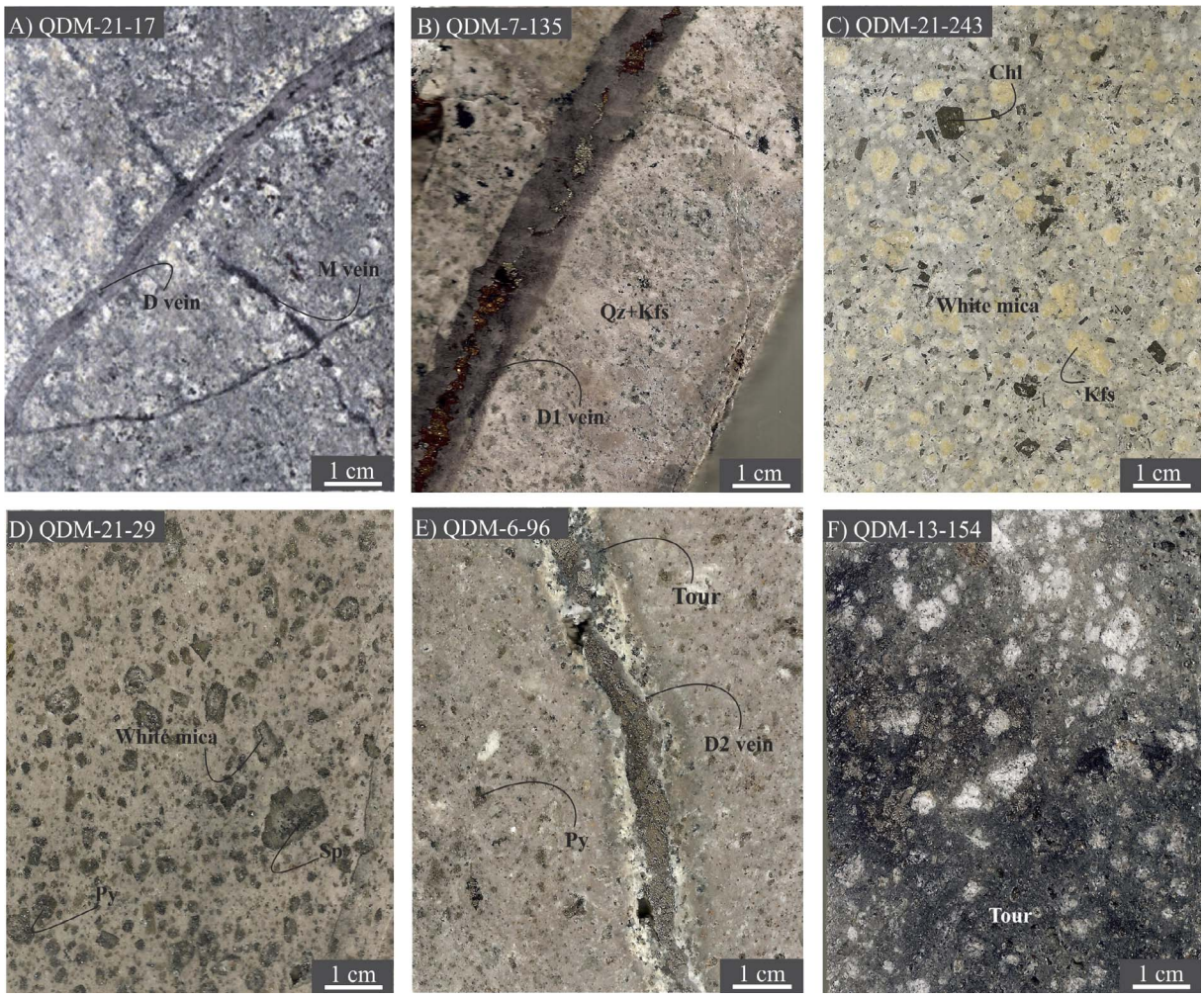

Fig. 3. Representative rock samples of QDM hydrothermal alteration types and veins. (A) M vein cut by D vein in QDM porphyry. (B) D1 vein in QDM porphyry affected by potassic alteration. (C) QDM porphyry affected by propylitic alteration with relict K-feldspar and superposed white mica. (D) QDM porphyry with phyllic alteration and pyrite-sphalerite mineralization. (E) D2 vein with white mica halo cut the QDM porphyry affected by phyllic alteration. (F) QDM porphyry affected by tourmaline-rich phyllic alteration.

(r = 0.10–0.15) and weak to null correlation with the rest of the metals (Table 3). In the phyllic segment of drill-hole QDM-021, representative of the shallow rich Au zones (Fig. 2, Table 3), Au exhibits a high positive correlation with Ag (r = 0.78), moderate positive correlation with Fe (r = 0.56) and weak correlation with As (r = 0.35), Zn (r = 0.16), Sb (r = 0.18) and Pb (r = –0.20), and does not correlate with Cu (r = 0.06) and Mn (r = –0.09).

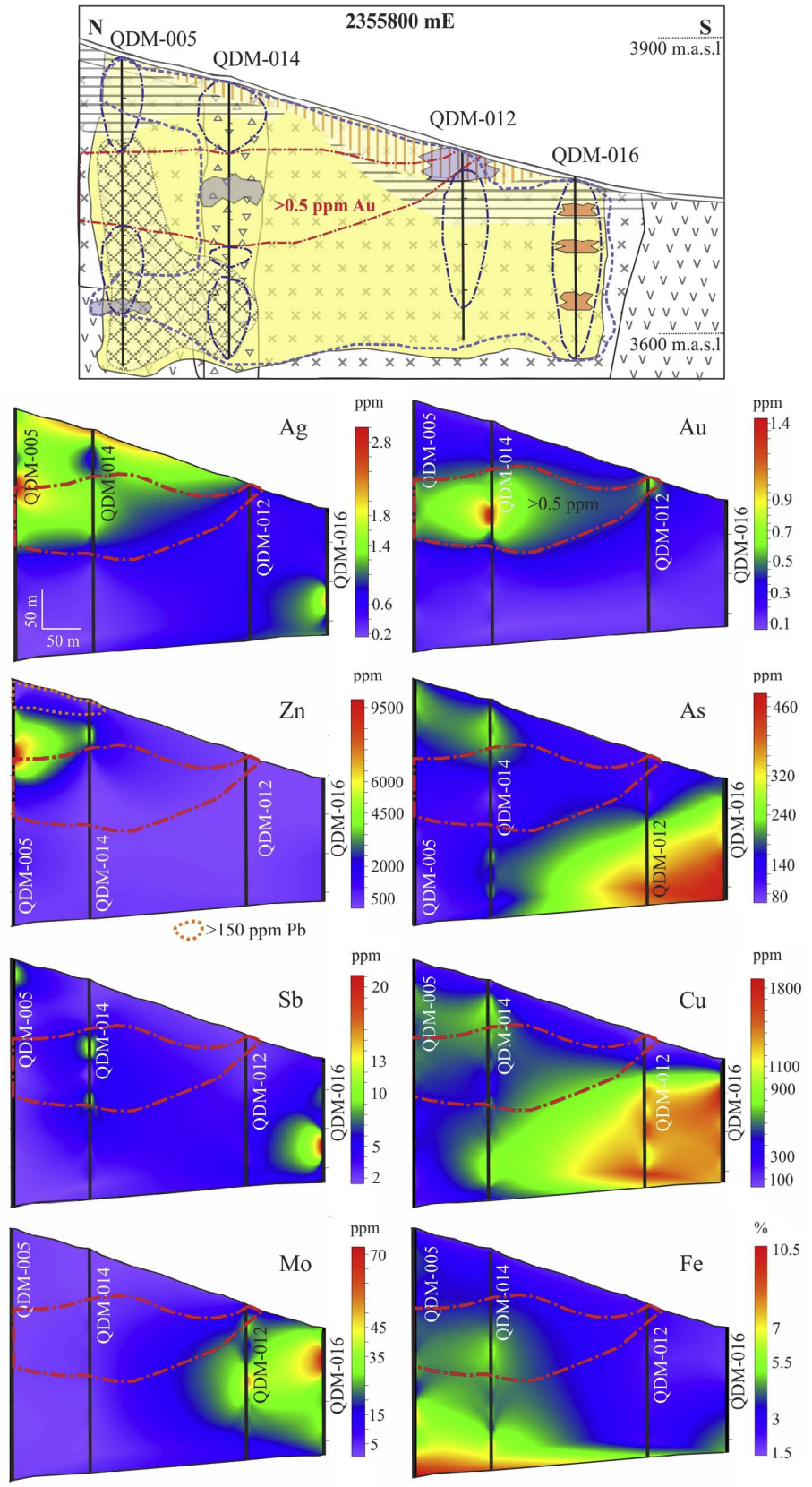

Fig. 4. Metals distribution in the North-South 2355800 mE section. Values of Pb higher than150 ppm occur above 3800 m.a.s.l.

6. Phyllosilicates mineralogy and composition

6.1. Chlorite

Chlorite was identified with optic microscopy, XRD, and microprobe analyses. Chlorite occurs as light-green sheetlike aggregates (< 20 μm) replacing amphibole and biotite phenocrysts and disseminated in the groundmass of the QDM porphyry. Chlorite was identified from the 001, 002, 003, and 004 reflections corresponding to d-spacing at 14.0–14.2, 7.07 to 7.09, 4.72 to 4.746, and 3.53 to 3.54 Å, respectively,

Table 3
Pearson correlation coefficients between Au and other metals in Quebrada de la Mina.

	Section 6517700 mN Au	Drill hole QDM 021* Au	Section 6517600 mN Au	Section 2355800 mE Au
Cu	0.22	0.07	−0.09	−0.05
Mo	−0.02	0.00	−0.14	−0.14
Ag	0.60	0.79	0.53	0.33
As	0.16	0.35	0.02	−0.15
Mn	−0.05	−0.09	−0.12	−0.14
Pb	−0.09	−0.21	−0.10	−0.12
Sb	0.22	0.19	−0.07	0.00
Zn	0.22	0.17	−0.04	0.02
Fe	0.13	0.56	0.15	0.10

*Geochemical analyses from the phyllic zone of drill hole QDM 021 (0–200 m)

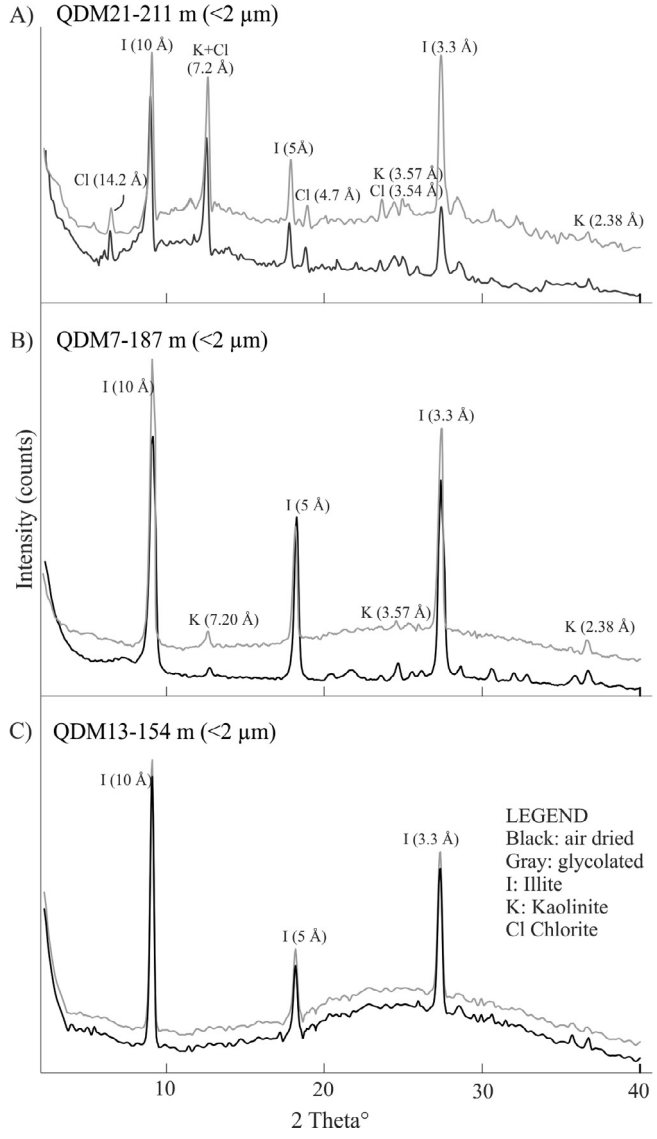

Fig. 5. Comparative analysis of the X-ray difraction (XRD) patterns in samples with layers clay minerals. (A) X-ray diffraction patterns for QDM21- 211 m (< 2 µm), with (I) illite, (K) kaolinite, and (Cl) chlorite. (B) X-ray diffraction patterns for QDM7- 187 m (< 2 µm), with (I) illite and (K) kaolinite. (C). X-ray diffraction patterns for QDM13-154 m (< 2 µm), with (I) illite.

in air-dried samples as well as after ethylene glycol saturation (Fig. 5A).

Table 1 summarizes the chemical composition of hydrothermal chlorites that occur in the propylitic alteration. In this study, the structural formula of chlorites was recalculated based on $O_{20}(OH)_{16}$ anions content (Newman and Brown, 1987), and all the iron was calculated as Fe^{2+} (Foster, 1962). Microprobe analyses of representative chlorite crystals from the propylitic alteration have the compositional range $(Al_{2.57–3.51}\ Mg_{4.14–5.56}\ Fe^{2+}_{2.70–3.59}\ (Si_{5.61–6.13}Al_{1.87–2.39})\ O_{20}\ (OH)_{16}$. Based on these ranges, the tetrahedral cation composition is between $(Si_{6.13}\ Al_{1.87})$ and $(Si_{5.61}\ Al_{2.39})$, and the octahedral cation totals are between 10.74 and 11.74 per $O_{20}\ (OH)_{16}$ formula unit. Thus, all are trioctahedral chlorites (Foster, 1962; Newman and Brown, 1987; Wiewióra and Weiss, 1990).

The chlorites are classified according to their dominant divalent cation, following the recommendations of Bayliss (1975), the AIPEA Nomenclature Subcommittee on chlorite (Bailey, 1980), and McLeod and Stanton (1984) are followed. The diagram of $Fe^{2+}/(Fe^{2+} + Mg)$ versus Si content (Fig. 6A) illustrates the range of chlorite solid solution in both Si-Al and Mg-Fe. All samples plot in the clinochlore field (Bayliss, 1975; Bailey, 1980; McLeod and Stanton, 1984; Wiewióra and Weiss, 1990). Fig. 6B and C presents the Fe versus Mg contents and the Al_2O_3 versus *X*Fe ratios for chlorites from the QDM project. Chlorites from Quebrada de la Mina have high contents of Mn (0.17–0.25 apfu) and Fe (2.70–3.59 apfu; Table 1). Chlorite from samples with propylitic alteration farthest from the phyllic alteration halo has higher Fe contents (sample QDM-021-243 m depth) and a slight decrease in Mn contents (Figs. 6, 7, Table 1).

Chlorite crystallization temperatures were estimated from the equations of Cathelineau (1988), considering that the Fe/(Fe + Mg) ratios of the studied chlorites are restricted to a range of 0.37 to 0.46. Even if chlorite geothermometry is based on empirical observations only, and not equilibrium reactions (Essene and Peacor, 1995), its use suggests temperatures between 258 and 322 °C for the propylitic alteration (Table 1).

6.2. White mica

White micas were identified under the microscope and microprobe analysis. White mica (> 2 µm) are overprinted in the potassic and propylitic alteration types, and are in equilibrium with phyllic and tourmaline rich-phyllic alteration types. In thin section white mica appears as coarse grained, colorless sheets (30–40 µm) replacing plagioglase phenocrysts and as very fine crystals (< 20 µm) disseminated in the groundmass of the QDM porphyry.

EPMA data of white micas were recalculated to atoms per formula unit (apfu), based on 11 oxygen atoms and all iron was considered as Fe^{2+}. The analytical results from 138 microprobe analyses for white micas (summarized in Table 2) are: $(K_{0.93–0.73}Na_{0.09–0.01}Ca_{0.01-0.00})_{0.77–0.98}\ (Al_{1.95–1.53}\ Mg_{0.35–0.03}\ Fe_{0.22–0.02}\ Mn_{0.01-0.00}\ Ti_{0.03–0.00})_{2.17–1.84}\ (Si_{3.36\ –3.07}\ Al_{0.93–0.64})\ (OHF_{0.09–0.00}Cl_{0.01–0.00})_2$. All analyzed white micas have less K and Na and more Si than theoretical dioctahedral micas (muscovite or phengite). The interlayer cation site occupancy (K + Na + Ca) varies from 0.77 to 0.98 apfu (Table 2). Most of the structural formulas display an unusually high octahedral occupancy (up to 2.17), which seems to be due to a slight excess of aluminum between 1.53 and 1.95.

In Fig. 8 (Velde, 1985), most white micas (> 2 µm) present in the propylitic, potassic, phyllic, tourmaline-rich phyllic, and phyllic haloes of D veins plot in the field of illite. White micas from the tourmaline-rich phyllic and from the phyllic haloes of D veins plot closer to the composition of muscovite (Fig. 8). In the muscovite-celadonite-pyrophyllite triangular coordinates (Fig. 9; Newman and Brown, 1987), white micas from all analyzed alterations plot between the composition of muscovite and the field of illite.

White micas from QDM show variations in the contents of Fe and Mg in the octahedral site; the Mg content varies from 0.03 to 0.35 apfu

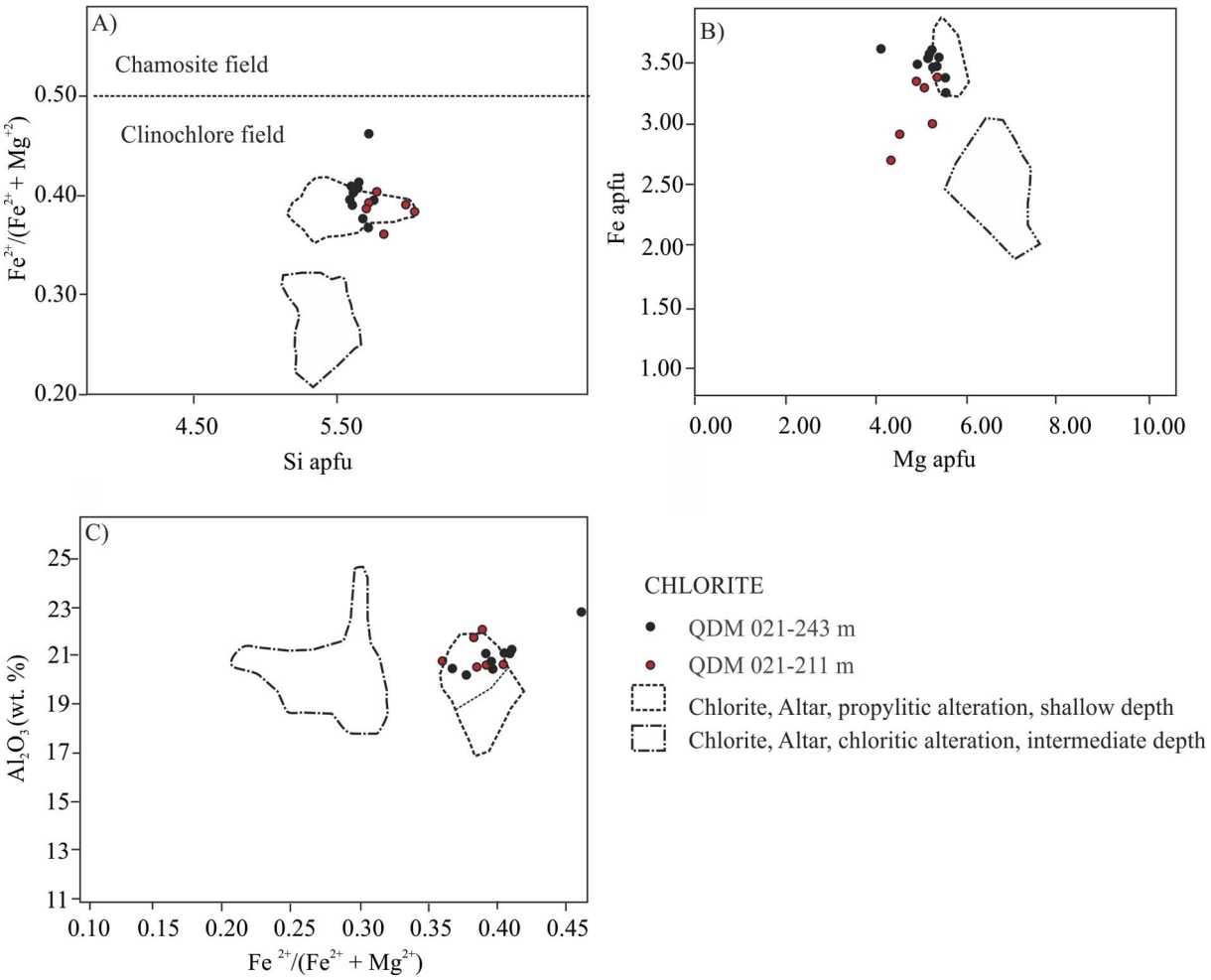

Fig. 6. Compositions of chlorite from QDM. (A) Fe/(Fe + Mg) versus Si (apfu), classified according to Bailey (1980) and McLeod and Stanton (1984). (B) Fe versus Mg (apfu), C) Al_2O_3 (wt%) versus Fe/(Fe + Mg). Chlorites from the Altar deposit are shown for comparison.

and the Fe contents between 0.02 and 0.22 apfu (Table 2). These variations can be recognized in Fig. 10 that shows the composition of the white micas from Deer et al. (1966) and Bailey (1984). White micas from samples with phyllic alteration and phyllic halos of D veins show values of Fe + Mg + Mn between 0.35 and 0.15 apfu and total Al (apfu) between 2.45 and 2.7. White micas from the tourmaline-rich phyllic alteration show the lowest values of Fe + Mg + Mn (0.11–0.05 apfu) and Al total between 2.8–2.85 apfu Table 2; Fig. 10). White micas from samples with propylitic and potassic alteration types show values of Fe + Mg + Mn between 0.40 and 0.55 (Table 2) and Al total contents between 2.40 and 2.55 apfu (Fig. 10). Compositional variations in white micas of QDM can be described by: (1) phengitic or Tschermak substitution $Al^{3+(VI)} + Al^{3+(IV)} <-> (Fe^{2+}, Mg^{2+})^{VI} + Si^{4+(IV)}$, (2) direct $Fe^{3+(VI)} <-> Al^{3+(VI)}$ substitution (Fig. 10), and (3) illitic substitution $(K^+)^{interlayer\ cation\ site} + Al^{3+(IV)} <-> Si^{4+(IV)} + []^{interlayer\ cation\ site}$ (Figs. 8, 9).

6.3. Clay minerals

6.3.1. Illite

Illite was distinguished by XRD in the < 2 μm fraction of the 20 analyzed samples and it is the most abundant clay mineral in the QDM deposit (Table 4). Illite was distinguished in air-dried, ethylene glycol-saturated, and calcinated samples by the sharp reflection of the 001 peak at 10 Å, and by rational 2nd, 3rd, and 4 th order reflections in 5, 3.3, and 2.5 Å (Fig. 5A, B, C).

The Kübler index of illite (illite crystallinity) in the clay-size fraction of the samples analyzed ranges from 0.27 to 0.1° 2θ (Table 4). Within the deposit, illite crystallinity increases with depth in the drill holes (Table 4).

6.3.2. Kaolinite

Kaolinite identification was based on data of XRD and infrared spectroscopy.

Kaolinite was distinguished by XRD in oriented aggregates air dried and glycolated by the sharp reflection of the 001 peak at 7.20 Å, for the 002 peak at 3.57 Å and for the 003 peak at 2.38 Å (Fig. 5A, B). In infrared spectroscopy, the diagnostic bands of kaolinite in the hydroxyl-stretching band region of phyllosilicates (i.e., 3500–3800 cm^{-1}) are 3695, 3668, 3652 and 3621 cm^{-1} (e.g., Madejová et al., 2011, Digital Appendix). Kaolinite crystallinity (FWHM, 2q, Table 4) in six samples analyzed show homogeneous values between 0.26 and 0.20.

6.4. Clay minerals and metals distribution

In the potassic assemblage the clay fraction represents ~40 vol% and corresponds to illite and subordinate kaolinite (Table 4). In the propylitic assemblage, the clay fraction represents between 23 to 43 vol % and consists of illite + chlorite + kaolinite. In samples with phyllic and tourmaline- rich phyllic assemblages, the clay fraction represents between 33 and 60 vol% and consists mainly of illite, sometimes accompanied by traces of kaolinite. In samples with phyllic haloes of D

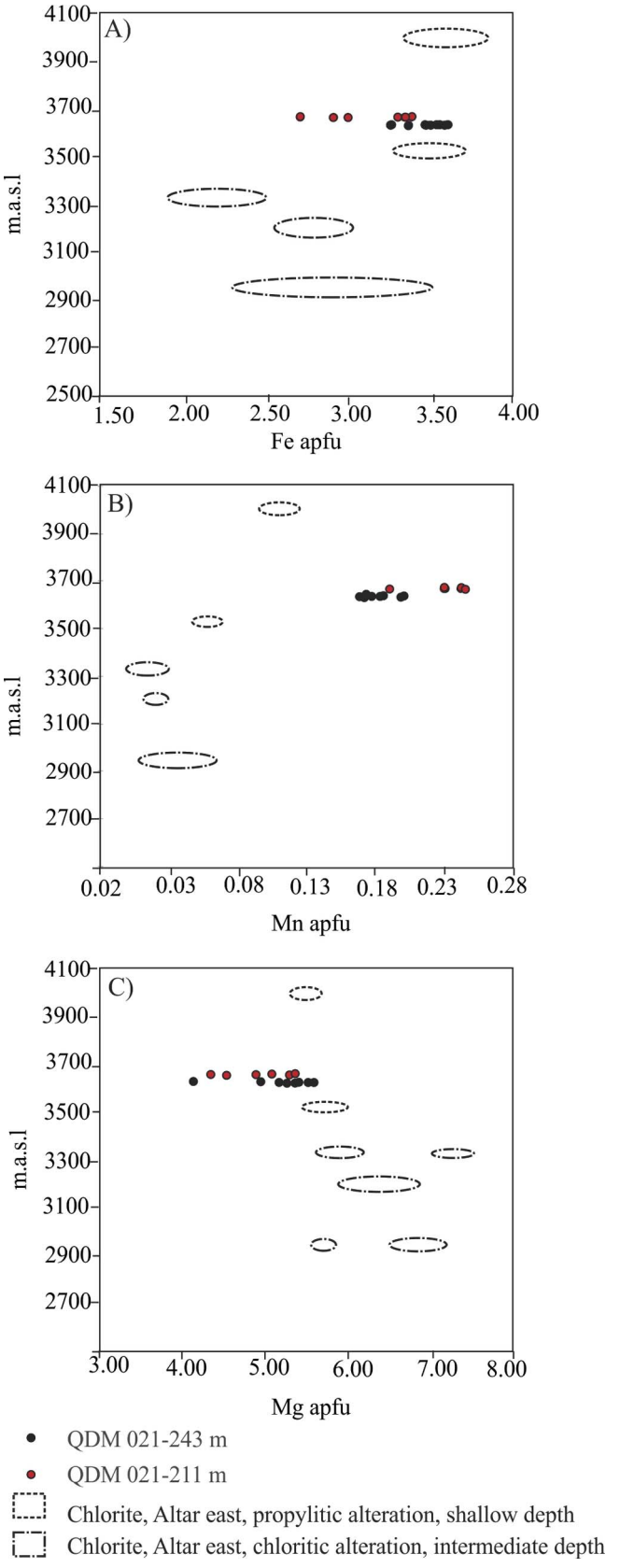

Fig. 7. Compositional variation in chlorites. Fe, Mn, and Mg (wt%) in chlorites from QDM are plotted versus m.a.s.l (meters above sea level). Chlorites from the Altar deposit are shown for comparison.

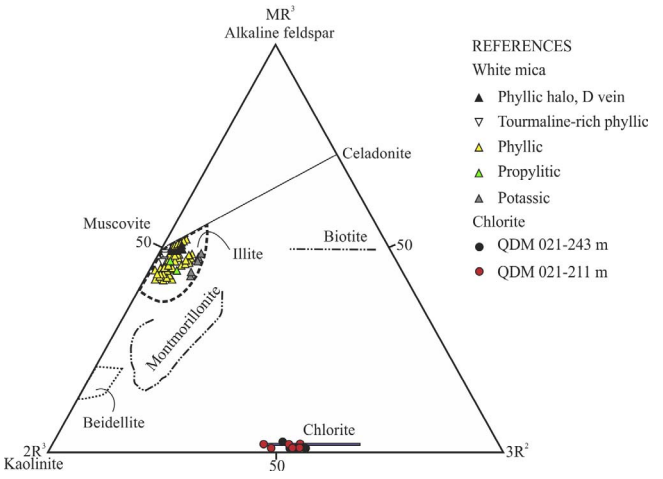

Fig. 8. Compositions of phyllosilicates at Quebrada de la Minawhere MR3 = Na + K + 2Ca; 2R3 = (Al + Fe^{3+}) − MR3)/2 and 3R2 = (Mg + Mn + Fe^{2+})/3 (Velde, 1985). Composition range of common phyllosilicates is indicated for comparison (Newman and Brown, 1987; Velde, 1985).

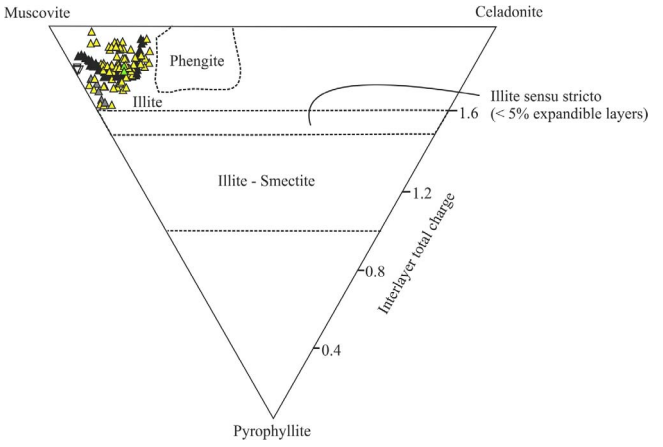

Fig. 9. Classification of white micas according to muscovite-celadonite-pyrophyllite end members (Newman and Brown, 1987).

veins the proportion of clays increases representing between 60 and 83 vol% and consists of illite with traces of kaolinite.

Most samples with the high grades of Au (> 0.5 ppm Au) have proportions of clay higher than 50 vol% that consist of illite and subordinate kaolinite. Samples from zones with low Au grades have a proportion of clay between 20 and 40 vol% that consists of chlorite, kaolinite and illite (Table 4).

7. Discussion

Shallow hydrothermal alteration zones of QDM are characterized by a phyllic halo that encompasses potassic alteration patches and is surrounded by an halo of propylitic alteration. Our study was focused on the the use of white micas, chlorite, and clay minerals present in the propylitic and phyllic zones of the porphyry deposit as monitors of the proximity to ore metals.

QDM shows typical alteration - mineralization features of porphyry deposits. *In situ* A veins were not observed and the scarse M and D veins recognized in core samples and outcrops reflect a low degree of erosion of the porphyry system.

7.1. Phyllosilicates

7.1.1. Propylitic alteration

We applied the empirical chlorite geothermometer of Cathelineau

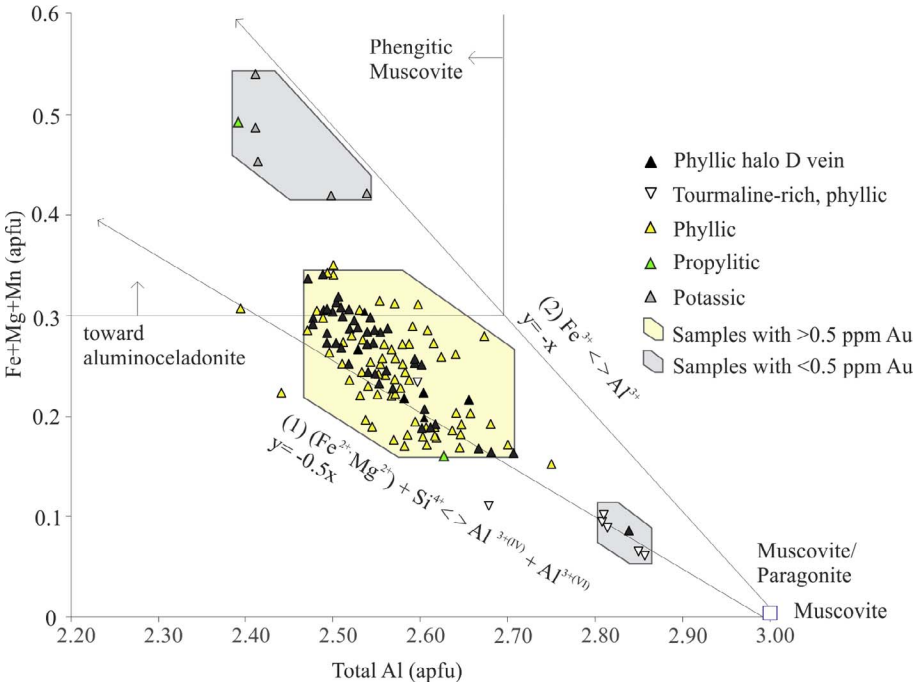

Fig. 10. Compositional variations of white micas in the Al (apfu) versus Fe + Mg + Mn (apfu) diagram (modified from Cohen, 2011). Arrows represent compositional vectors for main substitution mechanisms and symbols represent end-member compositions.

and Nieva (1985), based on the variation in the tetrahedral Al content within the chlorite structure (T (°C) = −61.92 + 321.98∗Al^{IV}) in chlorites from the propylitic alteration. The temperatures obtained range between 258° and 322° C (Table 1).

Chlorite (clinochlore) crystals from the propylitic zone of the QDM deposit show higher Fe and Mn and lower Mg contents compared to deeper chlorites from the nearby Altar Cu deposit associated with Cu mineralization (Altar chloritic alteration: Fe–apfu, Mg 5.7–7.41 apfu, Mn 0.01–0.03 apfu; Maydagán et al., 2016a). When compared to the chlorites from the Altar propylitic alteration, QDM chlorites have similar Fe contents, are enriched in Mn and impoverished in Mg (Altar propylitic alteration: Fe 3.3–3.7 apfu, Mg 5.4–5.6 apfu, Mn 0.10–0.12 apfu, Figs. 6 and 7; Maydagán et al. 2016a).

Wilkinson et al. (2015) showed that the propylitic alteration is not isochemical, rather, elements lost from the potassic zone are typically gained in the propylitic zone (e.g., Ca, Fe, and Co), and extensive outwards dispersion of other elements is observed.

These authors proposed that Mg in chlorites decreases exponentially in concentration with increasing distance from the mineralized center, whereas Mn and Fe show evidence for an enrichment halo, with peak concentrations at a distance of 1–1.5 km. Thus, high Mn and Fe contents observed in chlorites from the propylitic zone of the QDM could be indicative of the Mn and Fe enrichment halo, distant 1–1.5 km from the porphyry Cu-Au mineralized center. Recent drill-holes performed by the mining company have found a Cu-Au rich core at depth, which corroborates this hypothesis.

7.1.2. Phyllic and tourmaline rich phyllic alterations

In the center of the deposit, cooling of the hydrothermal fluids may have produced the pervasive phyllic alteration at QDM that overprinted the early hydrothermal assemblages and filled D veins with phyllic halos and straight-walls. Microthermometry of fluid inclusions combined with the titanium traces in quartz of D veins from the nearby Altar deposit suggests temperatures between 370 °C and 425° under hydrostatic pressures (Maydagán et al. 2015). These authors used the intersection of the minimum and maximum Ti-in-quartz isopleths (Huang and Audétat, 2012) with the corresponding fluid inclusion isochores to estimate the pressure and temperature of vein formation.

The composition of white micas (> 2 μm) from several porphyry copper deposits form a trend from near stoichiometric muscovite toward lower K + Na and higher Si, corresponding with ideal illite and beyond ideal illite, to higher Si and lower K + Na (Parry et al., 1984; 2002; Fig. 11). The punctual analyses of white micas of the phyllic alteration from QDM plot in the same compositional trend as those from other porphyry copper deposits worldwide, between muscovite and illite composition (Fig. 11, Parry et al., 2002; Franchini et al., 2012).

Hemley (1959) analyzed the hydrothermal alteration assemblages for the K_2O-Al_2O_3-SiO_2-KCl-HCl-H_2O system at 1.0 kbar with quartz present as a function of K+/H + versus temperature (°C). According to this study, Al-rich white micas, as found in the tourmaline rich-phyllic alteration of QDM (Fig. 10), suggest zones of high fluid/rock ratios and acidic fluids. Al-poor and Fe-Mg-rich white micas, as found in the propylitic and K-feldspar + quartz alteration types of QDM, are stable in near neutral pH conditions, and a decrease of fluid/rock ratios (e.g., Beaufort and Meunier, 1983; Reyes, 1990; Dilles et al., 2000; Mercier-Langevin et al., 2014).

In the analyzed sector of QDM, gold mineralization is associated with micas with intermediate contents of Al and Fe, Mn, and Mg (Fig. 10). Thus, these ranges of compositions of mica (Al content between 2.45 and 2.70 apfu and Fe + Mg + Mn between 0.35 and 0.15 apfu) are indicative of the proximity to the zones of circulation of the fluids responsible for the gold mineralization in the shallow porphyry environment of QDM deposit.

Despite tourmaline can occur in several vein types and hydrothermal alterations types of porphyry copper systems, it is mainly associated with D veins and magmatic-hydrothermal breccias affected by phyllic alteration (Sillitoe, 2010). The tourmaline-rich phyllic assemblage of QDM is interpreted as indicative of relatively late and low-temperature circulation of hydrothermal fluid connected with the late breccia and hydrothermal breccias with tourmaline cement that cut the QDM porphyry, during the final stages of the phyllic alteration. In QDM and Altar East (Maydagán et al., 2015), tourmaline is enriched in zones located above and around the potassic core, thus could be used as a mineral indicator to locate Cu cores at depth.

Gold mineralization (> 0.5 ppm Au) is also associated with high proportions of clays (> 50 vol%) that consist of illite and subordinate kaolinite. Illite, recognized in the clay fraction, may have been formed after the white micas, as the temperature of the hydrothermal fluids decreased to ~300 °C and represent a late and lower temperature stage of phyllic alteration (Simmons and Browne, 1998). The Kübler index

Table 4
Analysis performed with X-ray diffractometer.

Drill hole	Depth (m)	Hydrothermal assemblage	Sample mineralogy (vol%)	Fraction < 2 μm mineralogy (vol%)	FWHM (2q)	Illite crystallinity index	Au (ppm)*
QDM 006	32	Phyllic	Qz (64–66), Clay (30–32), pl (1 − 3), anh (1 − 3), py	Ilt		0.22	1.2
QDM 006	52	Phyllic	Clay (66–68), qz (28–30), kfs (2 − 4), anh (t), tour, py	Ilt		0.28	5.5
QDM 006	77	Phyllic, D vein	Clay (75–77), qz (18–20), anh (2 − 4), kfs (1 − 2), tour, py	ilt (94), kln (6)	0.24	0.12	1.4
QDM 006	78	Phyllic, D vein	Clay (55–57), qz (39–41), anh (2 − 4), kfs (t), py	Ilt, kln (t)		0.12	1.2
QDM 006	98	Phyllic, D vein	Clay (81–83), qz (17–19), kfs (t), py	Ilt, kln (t)		0.10	2.9
QDM 007	175	Propylitic	Qz (34–36), pl (27–29), Clay (23–25), cal (11–13), anh (1), kfs (t), py, hem, mag	.....		0.24	0.05
QDM 007	187	Potassic, Phyllic	Qz (52–54), clay (36–38), pl (2 − 4), anh (1 − 3), kfs (1 − 3), hem, mag, py (t)	Ilt (83), kln (17)	0.26	0.22	0.1
QDM 007	199.5	Potassic	Qz (41–42), clay (40–41), kfs (9 − 1 1), pl (6 − 8), anh (t), hem, py (t)	Ilt, kln (t)		0.19	0.06
QDM 011	68.6	Weak Phyllic	Qz (44–46), pl (27–29), clay (23–25), anh (1 − 3), gp (1), py	Ilt, kln (t)		0.22	0.5
QDM 011	95	Phyllic	Clay (50–52), qz (45–47), pl (1 − 2), anh (1), py, hem	Ilt, kln (t)		0.14	1.7
QDM 011	232	Phyllic	Clay (58–60), qz (34–36), pl (2 − 4), anh (1 − 2), py	Ilt, kln (t)		0.18	0.04
QDM 013	52	Phyllic	Qz (62–64), clay (31–33), pl (2 − 4), anh (1), py, tour	Ilt		0.20	2.0
QDM 013	154	Tourmaline-rich phyllic	Qz (64–66), clay (32–34), pl (2 − 4), anh (1), py, tour	Ilt		0.20	0.5
QDM 013	195	Phyllic	Clay (52–54), qz (39–41), pl (3 − 5), anh (1 − 3), py (t), tour	Ilt, kln (t)		0.12	0.07
QDM 021	24.2	Phyllic	Clay (44–46), pl (30–32), qz (23–25), anh (1), py, tour	kln (79), ilt (21), chl (t)	0.23	0.14	5.6
QDM 021	27.1	Phyllic	Qz (64–66), clay (33–35), pl (1 − 2), anh (t), py, tour	Ilt, kln (t)		0.15	0.6
QDM 021	30	Propylitic	Clay (41–43), qz (19–21), pl (12–14), gp (12–14), anh (1), py, tour	Ilt (71), chl (15), kln (14)	0.23	0.20	0.5
QDM 021	58	Phyllic	Qz (59–61), clay (39–41), pl (t), anh (t), py	Ilt, kln (t)		0.27	3.6
QDM 021	95.7	Phyllic	Clay (67–69), qz (27–29), pl (2 − 4), anh (1), py	Ilt, kln (t)		0.11	0.6
QDM 021	211	Propylitic	Clay (41–43), pl (38–40), qz (18–20), anh (1 − 3), py	Ilt (50), chl (35), kln (15)	0.21	0.17	0.03
QDM 021	243	Propylitic	Pl (53–55), clay (23–25), qz (19–21), anh (1 − 2), py	Ilt (65), chl (22), kln (13)	0.20	0.15	0.1

Abbreviations: anh: anhydrite; cal: calcite, clay: clay + mica; chl: chlorite, gp: gypsum, hem: hematite, ilt: Illite, kln: kaolinite, kfs: K-feldspar; mag: magnetite, pl: plagioclase, py: pyrite, qz: quartz, tour: tourmaline, t: traces.
Numbers in parentheses indicate the proportion determined by methods of quantification. FWHM (2q): kaolinite crystalinity. *Au (ppm) from drill-hole geochemical analyses.

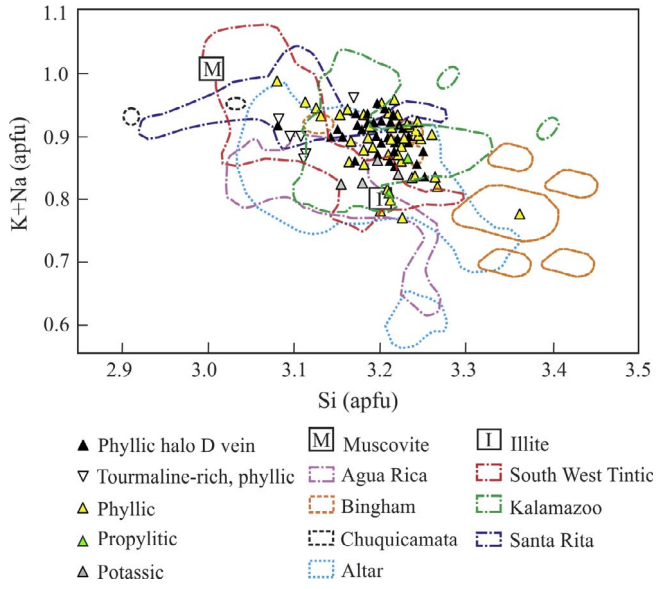

Fig. 11. Na + K versus Si for QDM white micas compared to the phyllosilicates from Altar (Maydagán et al., 2016a); Bingham, Chuquicamata and Kalamazoo (Guilbert and Schafer, 1979), Santa Rita, Binghamand Tintic southwest (Parry et al., 2002), Silbert (Beaufort and Meunier, 1983), and Agua Rica (Franchini et al., 2011).

values of illite from 0.1 to 0.19 2θ in deep samples from the drill cores (Table 4), are indicative of higher temperature and/or higher fluid/rock ratios during illite formation (Duba and Williams-Jones, 1983; Williams-Jones, 1986; Panno and Moore, 1994). Values of Kübler index of illite from 0.2 to 0.28 2θ in shallow samples from the drill holes are interpreted to reflect decreasing illity cristallinity, temperature of the fluids and fluid/rock ratio (e.g., Franchini et al., 2007; Table 4).

7.1.3. Late argillic alteration

Kaolinite occurs at deep and shallow sectors, is poorly developed and generally overlaps zones with phyllic alteration. Hydrothermal fluids with lower temperature and pH should have caused hydrolysis and the leaching of the alkali phyllosilicate cations. The temperature should have dropped below 200 °C with a pH of the fluid < 4 (Reyes, 1990, Table 4).

7.2. Metal zoning

Classical studies of hypogene metal and mineralogical zoning proposed two gold zones in porphyry deposits, one in the central copper orebody, and another peripheral to the copper zone that overlapped the lead-zinc mineralization (Emmons et al., 1927). In a later review, Jerome (1966) outlined a gold-enriched porphyry copper ore body, surrounded by a pyrite halo with lead-zinc-silver-manganese mineralization roughly encircling the pyrite zone. Jones (1992) examined the gold distribution in known gold-bearing porphyry copper systems and defined four categories of gold-bearing porphyry copper systems: (1) a central copper-gold zone; (2) an intermediate gold zone; (3) a distal gold zone; and (4) multiple gold zones. The intermediate gold zone consists of gold mineralization in an intermediate position between the central copper zone and the lead-zinc zone of porphyry copper districts that mostly occur within the pyrite halo (e.g., Neuerburg, 1978; Sillitoe, 1983, 1988; Sillitoe and Bonham, 1990).

The metal zoning in QDM is only weakly affected by supergene alteration. The analysis of the N–S section, which allows to observe the behavior of the metals between 3600 and 3900 m.a.s.l (Fig. 4), suggests that the gold-rich zone at shallow levels of QDM deposit may represent an intermediate gold zone occurring bellow a Ag-Zn-Pb-As zone and above a deeper Cu (Au, Mo) core.

At shallow levels, Au, Ag, Zn, As, and Pb precipitated forming haloes that partially overlapped in response to the decrease of fluid temperature from the center of the deposit to the periphery (e.g., Hemley and Hunt, 1992). The values of As in deep zones can be explained by the presence of traces of tennantite (or enargite) replacing early chalcopyrite and linked to late fluids. The study of QDM samples indicates that most of the gold in shallow levels of QDM coincides with pyrite in veins (D2 veins) and disseminations.

There are few descriptions of the intermediate gold zones in the scientific literature, thus we present a model that summarize the distribution of the alteration types in the shallow porphyry environment, disseminated sulfides, and their link with metals distribution which may be useful in mining exploration activities in porphyry deposits (Fig. 12).

We argue that in the shallow levels of QDM analyzed, during the phyllic alteration stage Au should have precipitated by the destabilization of sulfide complexes from the hydrothermal fluid and was incorporated into pyrite. The mechanisms of precipitation of pyrite with gold may be linked to cooling of the fluid and reaction with andesitic Fe-rich wall rocks that may increase their pH and supply Fe^{2+} favoring pyrite precipitation (e.g., Heinrich, 2005; Fontboté et al., 2017). Fig. 12

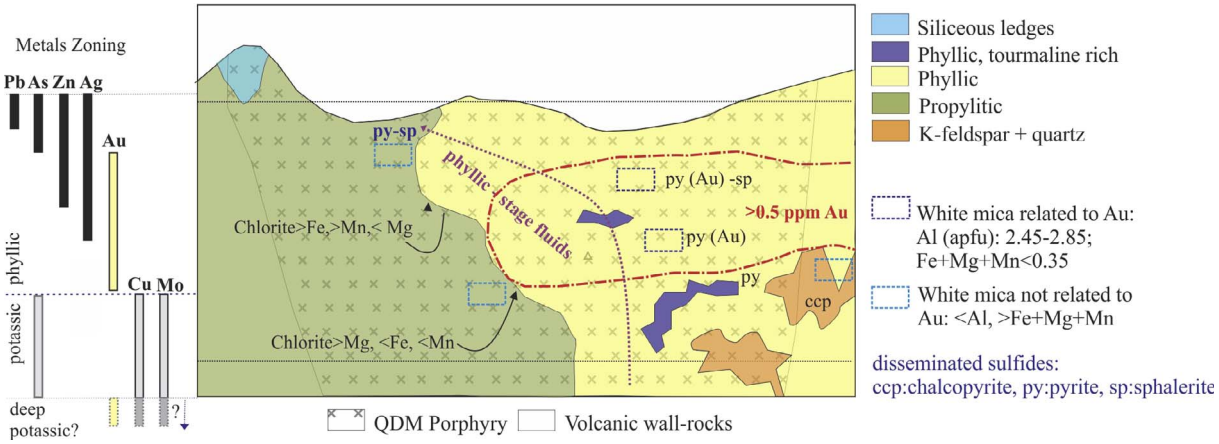

Fig. 12. Schematic model of the distribution of lithologies, hydrothermal alteration types, sulfides and metals zoning with depth in the shallow porphyry levels analyzed and transition to epithermal levels. The variation in the geochemistry of white mica and chlorite, and the zoning of metals and distribution of phyllosilicates in shallow porphyry levels is also shown.

summarize the variations in phyllosilicate geochemistry and distribution recognized in this study.

8. Conclusions

We present a study of the phyllosilicates and metals distribution in the propylitic and phyllic alteration zones of the Quebrada de la Mina porphyry Cu-Au deposit located in the Andean Main Cordillera of San Juan Province (Argentina) that represents a shallow porphyry environment.

The shallow gold-rich zone with sub-horizontal distribution at Quebrada de la Mina represents an example of an "Intermediate Gold Zone". These zones may indicate the presence of Cu (Au) mineralized cores at greater depth in porphyry systems.

Most of the gold mineralization at shallow levels of QDM is linked to pyrite in white micas zones (phyllic zones). Gold-rich zones have a high proportion of pyrite that may be the main carrier of gold.

High contents of Mn and Fe observed in chlorites (clinochlore) from peripheral QDM propylitic alteration could indicate the Mn enrichment halo recognized at distances of 1–1.5 km from the porphyry copper (gold) mineralized center.

Tourmaline appears in phyllic zones located above and around the potassic zones, thus could be used as an indicator to locate Cu cores at depth.

The compositional variations observed in white micas from the different alteration zones might have potential for mining exploration, as mica-like phyllosilicates with intermediate content of Fe, Mg and Mn and intermediate contents of Al occur in the highest gold grade zones.

Acknowledgments

This work forms part of a project financed by CONICET (PIP n° 330) and UN Comahue (PI n°: 04-I209). Part of this investigation was carried out in the Department of Geosciences, Oregon State University USU, Oregon, USA, through an International Cooperation Program directed by Dra Marta Franchini in Argentina, and Dr John Dilles in USA, and financed by CONICET (Argentina) and NSF (USA). David Lentz is supported by a NSERC Discovery grant. We express our appreciation to Roger Rey and Ralph Green for their support to this study, and to María Isabel Romero and all the staff of Peregrine Argentina S.A. for provision of site access, logistic support and help during the field work. We thank Noelia Di Giussepe and Lucas Riffo for their help during the field mapping and sampling.

Appendix A. Supplementary data

Supplementary data associated with this article can be found, in the online version, at http://dx.doi.org/10.1016/j.oregeorev.2017.11.028.

References

Anderson, M., Alvarado, P., Zandt, G., Beck, S., 2007. Geometry and brittle deformation of the subducting Nazca plate, central Chile and Argentina. Geophys. J. Int. 171, 419–434.
Bailey, S.W., 1980. Summary and recommendations of AIPEA Nomenclature Committee. Clays Clay Miner. 28, 73–78.
Bailey, S.W., 1984. Crystal chemistry of the true micas. Rev. Mineral. Geochem. 13, 13–60.
Bayliss, P., 1975. Nomenclature of the trioctahedral chlorites. Can. Mineral. 13, 178–180.
Beaufort, D., Meunier, A., 1983. A petrographic study of phyllic alteration superimposed on potassic alteration: the Sibert porphyry deposit. Econ. Geol. 78, 1514–1527.
Cahill, T., Isacks, B., 1992. Seismicity and shape of the subducted Nazca plate. J. Geophys. Res. 97, 17503–17529.
Cathelineau, M., 1988. Cation site occupancy in chlorites and illites as a function of temperature. Clay Miner. 23, 421–485.
Cathelineau, M., Nieva, D., 1985. A chlorite solid solution geothermometer. The Los Azufres (Mexico) geotermal system. Mineral. Petrol. 91, 235–244.
Charrier, R., Baeza, O., Elgueta, S., Flynn, J.J., Gans, P., Kay, S.M., Muñoz, N., Wyss, A.R., Zurita, E., 2002. Evidence for Cenozoic extensional basin development and tectonic inversion south of the flat-slab segment, southern Central Andes, Chile (33°–36° S). J. S. Am. Earth Sci. 15, 117–139.
Cohen, J.F., 2011. Mineralogy and geochemistry of hydrothermal alteration at the Ann-Mason porphyry copper deposit, Nevada: comparison of large-scale ore exploration techniques to mineral chemistry. Oregon State University, Oregon, USA, unpublished Master Thesis, p. 111.
Cooke, D.R., Baker, M., Hollings, P., Sweet, G., Chang, Z., Danyushevsky, Gilbert, S., Zhou, T., White, N., Gemmell, B., Inglis, S., 2014. New advances in detecting the distal geochemical footprints of porphyry systems—epidote mineral chemistry as a tool for vectoring and fertility assessments. Soc. Econ. Geol. Spec. Publ. 18, 127–152.
Deer, W.A., Howie, R.A., Zussman, J., 1966. An Introduction to the Rock Forming Minerals. Longman, London, pp. 528p.
Dilles, J.H., Einaudi, M.T., 1992. Wall-rock alteration and hydrothermal flow paths about the Ann-Mason porphyry copper deposit, Nevada—a 6-km vertical reconstruction. Econ. Geol. 87, 1963–2001.
Dilles, J.H., Proffett, J.M., Einaudi, M.T., 2000. Magmatic and hydrothermal features of the Yerington batholith with emphasis on the porphyry Cu(Mo) deposit in the Ann-Mason area. Soc. Econ. Geol. Guidebook Ser. 32, 67–89.
Duba, D., Williams-Jones, A., 1983. The application of illite crystallinity, organic matter reflectance, and isotopic techniques to mineral exploration: a case study in south-western Gaspé, Quebec. Econ. Geol. 78, 1350–1363.
Emmons, S.F., Irving, J.D., Loughlin, G.F., 1927. Geology and ore deposits of the Leadville mining district Colorado. US Government Printing Office, Professional Paper 148, 368p.
Essene, E.J., Peacor, D.R., 1995. Clay minerals thermometry—a critical perspective. Clays Clay Miner. 43, 540–553.
Fontboté, L., Kouzmanov, K., Chiaradia, M., Pokrovski, G.S., 2017. Sulfide minerals in hydrothermal deposits. Elements 13, 97–103.
Foster, M.D., 1962. Interpretation of the composition and a classification of the chlorites. U.S Geological Survey Professional Paper 414A, p. 33.
Franchini, M., Impiccini, A., Meinert, L., Grathoff, G., Schalamuk, I.B., 2007. Clay mineralogy and zonation in the Campana Mahuida porphyry Cu deposit, Neuquén, Argentina: implications for porphyry Cu exploration. Econ. Geol. 102, 27–54.
Franchini, M., Impiccini, A., Lentz, D., Ríos, F.J., O'Leary, S., Pons, J., Schalamuk, A.I., 2011. Porphyry to epithermal transition in the Agua Rica polymetallic deposit, Catamarca, Argentina: an integrated petrologic analysis of ore and alteration parageneses. Ore Geol. Rev. 41 (1), 49–74.
Franchini, M., Impiccini, A., Beaufort, D., Patrier, P., Anderson, C.G., Pons, J., 2012. Mineral assemblages and distribution of phyllosilicates composition along the main section of the Agua Rica deposit, Catamarca, Argentina: implications for future mine development. Appl. Clay Sci. 67, 61–71.
Gans, C.R., Beck, S.L., Zandt, G., Gilbert, H., Alvarado, P., Anderson, M., Linkimer, L., 2011. Continental and oceanic crustal structure of the Pampean flat slab region, western Argentina, using receiver function analysis: new high-resolution results. Geophys. J. Int. 186, 45–58.
Guggenheim, S., Bain, D.C., Bergaya, F., Brigatti, M.F., Drits, V.A., Eberl, D.D., Stanjek, H., 2002. Report of the Association Internationale pour l'Etude des Argiles (AIPEA) Nomenclature Committee for 2001: order, disorder and crystallinity in phyllosilicates and the use of the 'Crystallinity Index'. Clay Miner. 37 (2), 389–393.
Guilbert, J. M., Schafer, R. W., 1979. Preliminary geochemical characterization of muscovites in porphyry base-metal alteration assemblages. Nevada Bureau of Mines and Geology Report 33.
Gustafson, L.B., Hunt, J.P., 1975. The porphyry copper deposit al El Salvador, Chile. Econ. Geol. 70, 857–912.
Gustafson, L.B., Quiroga, J., 1995. Patterns of mineralization and alteration below the porphyry copper orebody at El Salvador, Chile. Econ. Geol. 90, 2–16.
Heinrich, C.A., 2005. The physical and chemical evolution of low-salinity magmatic fluids at the porphyry to epithermal transition: a thermodynamic study. Miner. Deposita 39, 864–889.
Hemley, J.J., 1959. Some mineralogical equilibria in the system K_2O-Al_2O_3-SiO_2-H_2O. Am. J. Sci. 257 (4), 241–270.
Hemley, J.J., Hunt, J.P., 1992. Hydrothermal ore-forming processes in the light of studies in rock-buffered systems; II, some general geologic applications. Econ. Geol. 87, 23–43.
Huang, R., Audétat, A., 2012. The titanium-in-quartz (TitaniQ) thermobarometer: a critical examination and re-calibration. Geochim. Cosmochim. Acta 84, 75–89.
Jerome, S.E., 1966. Some features pertinent in exploration of porphyry copper deposits. In: Titley, S.R., Hicks, C.L. (Eds.), Geology of the Porphyry Copper Deposits, Southwestern North America. University of Arizona Press, Tucson, AZ, pp. 75–85.
In, Z.J., Zhu, J., Ji, J., Li, F., Lu, X., 2002. Two origins of illite at the Dexing porphyry Cu deposit, East China: implications for ore-forming fluid constraint on illite crystallinity. Clays Clay Miner. 50 (3), 381–387.
Jones, B., 1992. Application of metal zoning to gold exploration in porphyry copper systems. J. Geochem. Explor. 43, 127–155.
Kay, S.M., Mpodozis, C., 2002. Magmatism as a probe to the Neogene shallowing of the Nazca plate beneath the modern Chilean flat-slab. J. S. Am. Earth Sci. 15, 39–57.
Kisch, H.J., 1991. Illite crystallinity: recommendations on sample preparation, X-ray diffraction settings, and interlaboratory samples. J. Metamorph. Geol. 9 (6), 665–670.
Klohn, C. 1960. Geología de la Cordillera de los Andes de Chile central, provincias de Santiago, O'Higgins, CoIchagua y Curicó. Instituto de Investigaciones Geológicas (Chile) 8, p. 95.
Kübler, B., 1964. Les argiles, indicateurs de métamorphisme: Revue de l'Institut Francaise du Petrole 19, 1093–1112.
Kübler, B., 1967. La cristallinité de l'illite et les zones tout à fait supérieures du métamorphisme. Etages Tectoniques: Switzerland, Neuchàtel University 105–121.
Lowell, J., Guilbert, J., 1970. Lateral and vertical alteration-mineral zoning in porphyry

ore deposits. Econ. Geol. 65, 373–408.
Masterman, G.J., Cooke, D.R., Berry, R.F., Walshe, J.L., Lee, A.W., Clark, A.H., 2005. Fluid chemistry, structural setting, and emplacement history of the Rosario Cu-Mo porphyry and Cu-Ag-Au epithermal veins, Collahuasi district, northern Chile. Econ. Geol. 100, 835–862.
Madejová, J., Balan, E., Petit, S., 2011. Application of vibrational spectroscopy to the characterization of phyllosilicates and other industrial minerals. Adv. Character. Ind. Min. EMU Notes Mineral. 9, 171–226.
Maydagán, L., Franchini, M., Chiaradia, M., Pons, J., Impiccini, A., Toohey, J., Rey, R., 2011. Petrology of the Miocene igneous rocks in the Altar Region, Main Cordillera of San Juan, Argentina: a geodynamic model within the context of the Andean flat-slab segment and metallogenesis. J. S. Am. Earth Sci. 32, 30–48.
Maydagán, L., 2012. El Prospecto de Cu-(Au-Mo) Altar (31° 29′LS, 70°28′LO), San Juan. Unpublished Ph.D thesis, Universidad Nacional del Sur, Bahía Blanca, Argentina, p. 340.
Maydagán, L., Franchini, M., Rusk, B., Lentz, D., McFarlane, C., Impiccini, A., Ríos, F.J., Rey, R., 2015. Porphyry to epithermal transition in the Altar Cu-(Au-Mo) Deposit, Argentina, studied by cathodoluminescence, LA-ICP-MS, and fluid inclusion analysis. Econ. Geol. 110, 889–923.
Maydagán, L., Franchini, M., Impiccini, A., Lentz, D., 2016. Phyllosilicates geochemistry and distribution in the Altar porphyry Cu-(Au) deposit, Andes Cordillera of San Juan, Argentina: applications in exploration, geothermometry, and geometallurgy. J. Geochem. Explor. 167, 83–109.
Maydagán, L., Franchini, M., Chiaradia, M., Bouhier, V., Di Giuseppe, N., Rey, R., Dimieri, L., 2016. Petrogenesis of Quebrada de la Mina and Altar North porphyries (Cordillera of San Juan, Argentina): crustal assimilation and metallogenic implications. Geosci. Front. 8, 1135–1159.
McLeod, R.L., Stanton, R.L., 1984. Phyllosilicates and associated minerals in some Paleozoic stratiform sulfide deposits of southeastern Australia. Econ. Geol. 79, 1–22.
Mercier-Langevin, P., Lafrance, B., Bécu, V., Dubé, B., Kjarsgaard, I., Guha, J., 2014. The Lemoine auriferous volcanogenic massive sulfide deposit, Chibougamau camp, Abitibi greenstone belt, Quebec, Canada: geology and genesis. Econ. Geol. 109, 231–269.
Meyer, C., Hemley, J.J., 1967. Wall rock alteration. In: Barnes H.L. (Ed.), 2nd ed. Geochemistry of Hydrothermal Ore Deposits. John Wiley & Sons, New York, p. 798.
Moore, D.M., Reynolds Jr., R.C., 1997. X-ray diffraction and the identification and analysis of clay minerals. Oxford University Press, New York, NY, pp. 155p.
Mpodozis, C., Brockway, H., Marquardt, C., Perelló, J., 2009. Geocronología U-Pb y tectónica de la región Los Pelambres-Cerro Mercedario: Implicancias para la evolución cenozoica de los Andes del centro de Chile y Argentina. XII Congreso Geológico Chileno, Santiago de Chile, 2009, Proceedings S9–059, p. 4.
Neuerburg, G.J., 1978. The architecture of the porphyry-metal system as a prospecting stratagem in the southern Rocky Mountains. U.S. Geol. Surv. Open File Rep. 33, 78–130.
Newman, A., Brown, G., 1987. The chemical constitution of clays. In: Newman, A. (Ed.). Chemistry of Clays and Clay Minerals: Mineralogical Society Monograph 6, pp. 1–129.
Panno, S.V., Moore, D.M., 1994. Mineralogy of the clay-sized fraction of the Davis Shale, Southeast Missouri; alteration associated with a mississippi valley-type ore deposit. Econ. Geol. 89, 333–340.
Parry, W.T., Ballantyne, J.M., Jacobs, D.C., 1984. Geochemistry of hydrothermal sericite from Roosevelt Hot Springs and the Tintic and Santa Rita porphyry copper systems. Econ. Geol. 79 (1), 72–86.
Parry, W., Jasumback, M., Wilson, P., 2002. Clay mineralogy of phyllic and intermediate argillic alteration at Bingham, Utah. Econ. Geol. 97, 221–239.
Pouchou, J.L., Pichoir, F., 1984. A new model for quantitative X-ray microanalyses, part I. Application to the analyses of homogenous samples. Rech. Aerospatiale 3, 13–36.
Reyes, A.G., 1990. Petrology of Philippines geothermal systems and the application of alteration mineralogy to their assessment. J. Volcanol. Geoth. Res. 43, 279–309.
Reynolds, R.C., Jr., Reynolds, R.C., III, 1996. NEWMOD©-for-Windows. The calculation of one dimensional X-ray diffraction patterns of mixed-layered clay minerals. Brook Road, Hanover, New Hampshire, R.C.
Sillitoe, R.H., 1983. Enargite-bearing massive sulfide deposits high in porphyry copper systems. Econ. Geol. 78, 348–352.
Sillitoe, R.H., 1988. Epochs of intrusion-related copper mineralization in the Andes. J. S. Am. Earth Sci. 1, 89–108.
Sillitoe, R.H., 2010. Porphyry copper systems. Econ. Geol. 105, 3–41.
Sillitoe, R.H., Bonham, H.F., 1990. Sediment-hosted gold deposits: distal products of magmatic-hydrothermal systems. Geology 18, 157–161.
Simmons, S.F., Browne, P.R.L., 1998. Illite, illite–smectite and smectite occurrences in the Broadlands-Ohaaki geothermal system and their implications for clay mineral geothermometry. Water Rock Interaction 9, 691–694.
Velde, B., 1985. Clay minerals: a physico-chemical explanation of their occurrence: developments in sedimentology 40. Elsevier, Amsterdam, Netherlands, pp. 427.
Wiewióra, A., Weiss, Z., 1990. Crystallochemical classifications of phyllosilicates based on the unified system of projection of chemical composition: II. The chlorite group. Clay Minerals 25, 83–92.
Wilkinson, J.J., Chang, Z., Cooke, D.R., Baker, M.J., Wilkinson, C.C., Inglis, S., Gemmell, J.B., 2015. The chlorite proximitor: a new tool for detecting porphyry ore deposits. J. Geochem. Explor. 152, 10–26.
Williams-Jones, A.E., 1986. Low-temperature metamorphism of the rocks surrounding les Mines Gaspe, Quebec; implications for mineral exploration. Econ. Geol. 81 (2), 466–470.